DETERMINATION OF ELECTRONIC PROPERTIES OF MATERIALS USING DIFFERENTIAL REFLECTOMETRY

By

Rosalia Josephine Nastasi

A DISSERTATION PRESENTED TO THE GRADUATE COUNCIL OF
THE UNIVERSITY OF FLORIDA
IN PARTIAL FULFILLMENT OF THE REQUIREMENTS FOR THE
DEGREE OF DOCTOR OF PHILOSOPHY

UNIVERSITY OF FLORIDA

1976

With great pride and love,
I would like to dedicate
this work to

My Parents,

whose unselfishness and
faith in me have helped
make it possible.

ACKNOWLEDGEMENTS

The author would like to express her sincere appreciation to her advisor, Dr. Rolf E. Hummel, for his unselfish donation of time and help throughout this investigation. Through his encouragement, friendship, and support, the author has grown both intellectually and personally.

Special thanks are extended to Dr. J. Barry Andrews for many interesting discussions and his design and construction of the differential reflectometer.

The valuable discussions with Drs. J. Connolly and R. T. DeHoff concerning the theory involved in this work are greatly appreciated.

Many thanks are also extended to Mr. C. Shanley for numerous stimulating discussions.

The author would also like to thank Mrs. Vicki Turner for her assistance in the preparation of this manuscript.

Thanks are also extended to Drs. J. J. Hren, R. Pepinsky, and D. B. Dove for serving on the author's supervisory committee.

The author is grateful to the Department of Materials Science and Engineering for financial support during this research.

TABLE OF CONTENTS

Page

ACKNOWLEDGMENTS....iii

LIST OF TABLES....vi

LIST OF FIGURES....viii

ABSTRACT....xiii

CHAPTER

I INTRODUCTION....1

II LITERATURE SURVEY....9
- II-1 General Remarks....9
- II-2 Pure Copper....13
- II-3 Copper Based Alloys....21
- II-4 Recent Results Using Modulation Techniques....31
- II-5 Summary....53

III EXPERIMENTAL PROCEDURE....61
- III-1 Sample Preparation....61
- III-2 Experimental Setup - The Differential Reflectometer....65

IV THEORETICAL BACKGROUND....68
- IV-1 Relationship of Optical Properties to Electronic Structure....68
- IV-2 Relationship of Differential Reflectograms With Interband Absorption....72
- IV-3 Line Shape Analysis....87

V EXPERIMENTAL RESULTS....99

TABLE OF CONTENTS - continued.

Page

CHAPTER

VI DATA ANALYSIS AND DISCUSSION....138
- VI-1 General Remarks....138
- VI-2 Threshold Energy of Interband Transitions....139
- VI-3 High Energy Structure in the Differential Reflectograms....154
  - VI-3.1 Transition Around 5 ev....154
  - VI-3.2 Transition Around 4 ev....161
- VI-4 Cu-Au Alloys....167
  - VI-4.1 General Remarks....167
  - VI-4.2 Threshold Energy for Interband Transitions....167
  - VI-4.3 Lower d-bands to Fermi Energy Transitions....168
  - VI-4.4 Conduction Band to Conduction Band Transitions....168
  - VI-4.5 Broad Structure....170

APPENDICES

1....174

2....175

BIBLIOGRAPHY....176

BIOGRAPHICAL SKETCH....179

LIST OF TABLES

Table Page

1.1 Elements Which Were Alloyed With Copper...........8

2.1 Experimental and Theoretical Results for Changes in Transition Energy from Cu to 30 at.% Zn.......................................22

2.2 Comparison of Peak Assignments of Cu-Zn Alloys.......................................22

2.3 Assignments of Structure in the Optical Spectra of Cu and Cu Alloys......................29

2.4 Identification of the Important Interband Transitions of Cu................................33

2.5 Assignment of Structure in the Optical Spectrum of Cu by Author.........................54

2.6 Assignment of Structure in the Optical Spectrum of Cu by Energy.........................57

3.1 Alloy Compositions Prepared in This Study........62

6.1a Uncorrected (Raw Data) and Corrected Values for Peak "A" as a Function of Composition for Cu-Zn Alloys...............................140

6.1b Uncorrected (Raw Data) and Corrected Values for Peak "A" as a Function of Composition for Cu-Al Alloys...............................141

6.1c Uncorrected (Raw Data) and Corrected Values for Peak "A" as a Function of Composition for Cu-Ga Alloys...............................142

6.1d Uncorrected (Raw Data) and Corrected Values for Peak "A" as a Function of Composition for Cu-Si Alloys...............................142

LIST OF TABLES - continued.

Table Page

6.1e Uncorrected (Raw Data) and Corrected Values for Peak "A" as a Function of Composition for Cu-Ge Alloys....143

6.1f Uncorrected (Raw Data) and Corrected Values for Peak "A" as a Function of Composition for Cu-Sn Alloys....144

6.1g Uncorrected (Raw Data) and Corrected Values for Peak "A" as a Function of Composition for Cu-As Alloys....144

6.2 Energy of Peak "D" and Shift in Energy as a Function of Composition for Various Copper Based Alloys....158

6.3a Energy of Peak "B" as a Function of Solute Concentration for Cu-Zn Alloys....164

6.3b Energy of Peak "B" as a Function of Solute Concentration for Cu-Al Alloys....164

6.3c Energy of Peak "B" as a Function of Solute Concentration for Cu-Ga Alloys....165

6.3d Energy of Peak "B" as a Function of Solute Concentration for Cu-Sn Alloys....165

LIST OF FIGURES

Figure Page

1.1 The reflectivity of copper in the wavelength range of 700 nm to 200 nm.............3

2.1 Optical Absorptivity of α-brasses in the ultraviolet and visible regions.............12

2.2 Energy Band Diagram of Copper..................14

2.3 Spectral Dependence of the absorption coefficient of Cu over the range 1 → 25 ev.......................................15

2.4 Plot of interband contribution to $\varepsilon_2(\omega)$ in the range $1.5 \leq \hbar\omega \leq 10$ ev for Cu............20

2.5 Energy dependence of ε_2 for Cu.................20

2.6 Comparison of energy bands of copper (solid lines) with those of Cu-30at.% Zn (dashed lines)............................24

2.7a Cu-Zn absorption spectrum at 295°K. Broken curve, pure copper; O Cu-Zn 16at.%; Δ Cu-Zn 27at.%; + Cu-Zn 32at.%..........26

2.7b Cu-Ga absorption spectrum at 295°K. Broken curve, pure copper; O Cu-Ga 6at.%; Δ Cu-Ga 8at.%; + Cu-Ga 12at.%; □ Cu-Ga 16at.%...............................26

2.7c Cu-Ge absorption spectrum at 295°K. Broken curve, pure copper; O Gu-Ge 4at.%; Δ Cu-Ge 8at.%..........................27

2.7d Cu-As absorption spectrum at 295°K. Broken curve, pure copper; O Cu-As 2at.%; Δ Cu-As 4at.%; + Cu-As 6.5at.%...........27

2.8 Experimental and calculated wavelength modulation curves for copper at T = 7°K.........32

LIST OF FIGURES - continued.

Figure Page

2.9 Derivative of Reflectivity with respect to energy of Cu at 80°K........................36

2.10 Imaginary part of the dielectric constant, ε_2, for Cu obtained at 80°K by a Kramers-Kronig analysis................................36

2.11 Experimental values of ε_2 for copper as a function of photon energy. Also included are the theoretical curves of Williams et al.[21] and Fong et al.[19]............38

2.12 Imaginary part of the dielectric function (ε_2) for Cu and for low concentration Cu-Al alloys at room temperature..................41

2.13 Energy bands of copper near the L symmetry point, showing the direct neck gap (4.3 ev), and the indirect neck gap (4.0 ev)..............41

2.14 Energy location of the observed onset of interconduction-band absorption as a function of solute concentration. Direct neck gap at low concentrations and indirect neck gap at high concentrations.................43

2.15 Thermotransmission and thermoreflection spectra of a 455 Å thick film of copper at 350 K. Open circles represent ΔT/T and closed circles ΔR/R........................44

2.16 $\Delta\varepsilon_2$ spectrum resulting from spectra in Figure 2.15..................................45

2.17 Experimental curves of α/c where $\alpha = \frac{(R_{pure}-R_{alloy})}{(R_{pure}+R_{alloy})}$ and c = average composition vs. photon energy for Cu-Au alloys...47

LIST OF FIGURES - continued.

Figure Page

2.18 Energy level diagram for pure crystals and α-Cu 30at.% Zn
(a) pure cyrstals and Neutral Atom model
(b) Neutral Atom, SMT, and CR models............52

3.1 Schematic Diagram of the optical and electronic components of the differential reflectometer..................................66

4.1 Transition $\Delta_5 \rightarrow \Delta_1$ corresponding to peak "A" in the differential reflectograms...........77

4.2a Fermi Distribution Function.....................79

4.2b Derivative of Fermi Distribution Function with respect to E_s..............................79

4.3 F(s) vs. s for Θ values from 0° to 330°.........86

4.4 Calculated F(s) curves as a function of s for Θ between 90 and 180° in increments of 5° 88 - 91

4.5 Plot of F(s) vs. s for a Θ value of 145°........93

4.6 Plot of $F(S'')/F(S_M)$ vs. Θ.....................94

4.7 Correction factor R as a function of Θ..........96

4.8 Differential Reflectogram of Cu-1at.% Al in the region of peak "A"......................97

5.1 Elements used in this study for alloying with copper (bold lines).......................100

5.2 Differential Reflectograms for various Cu-Zn alloys.................................. 102-104

5.3 Differential Reflectograms for various Cu-Al alloys..................................106-112

LIST OF FIGURES - continued.

Figure Page

5.4 Differential Reflectograms for various Cu-Ga alloys....114-116

5.5 Differential Reflectograms for various Cu-Ge alloys....118-120

5.6 Differential Reflectograms for various Cu-Si alloys....122-124

5.7 Differential Reflectograms for various Cu-Sn alloys....126-128

5.8 Differential Reflectograms for various Cu-As alloys....130-132

5.9 Differential Reflectograms for various Cu-Au alloys....134-136

6.1 Corrected transitional energies for peak "A" as a function of solute concentration for Cu-Zn, Cu-Al, Cu-Ga, Cu-Ge, Cu-Si, and Cu-Sn alloys.
a = possible error in marking maxima
b = possible error in line shape analysis......147

6.2 Uncorrected transitional energies (raw data) for peak "A" as a function of solute concentration for Cu-Zn, Cu-Al, Cu-Ga, Cu-Ge, Cu-Si, Cu-Sn, and Cu-As alloys.
a = possible error in marking maxima...........149

6.3 Plot of corrected transitional energies for peak "A" as a function of e/a ratio for Cu-Zn, Cu-Al, Cu-Ga, Cu-Ge, Cu-Si, Cu-Sn, and Cu-As alloys.
a = possible error in marking maxima...........151

6.4 The Seraphin coefficients α and β for copper.........155

LIST OF FIGURES - continued.

Figure Page

6.5 Energy of peak "D" and shift in energy compared to "pure copper" as a function of composition for various copper-based alloys....159

6.6 Energy of peaks "B" and "C" vs. solute concentration for Cu-Zn alloys....162

6.7 Energy of peak "B" and shift in energy compared to "pure copper" as a function of composition for various copper-based alloys....166

6.8 Energy of peak "b" as a function of composition for Cu-Au alloys. a = possible error in marking maxima....169

6.9 Energy of peak "d" as a function of composition for Cu-Au alloys....171

6.10 Energy of peak "c" as a function of composition for Cu-Au alloys....172

Abstract of Dissertation Presented to the
Graduate Council of the University of Florida
in Partial Fulfillment of the Requirements for the
Degree of Doctor of Philosophy

DETERMINATION OF ELECTRONIC PROPERTIES OF MATERIALS USING DIFFERENTIAL REFLECTOMETRY

By

Rosalia Josephine Nastasi

August, 1976

Chairman: Rolf E. Hummel
Major Department: Materials Science and Engineering

A systematic and comprehensive study of the optical properties of a large range of α-phase copper based alloys was undertaken. The solutes were selected to include elements with one, two, three, four, and five valence electrons, including Gold, Zinc, Aluminum, Gallium, Germanium, Silicon, Tin, and Arsenic.

The instrument used for this investigation was the differential reflectometer which is capable of determining within a few hundredths of an electron volt the energy for interband transitions of electrons.

Important parts of the line shape of the differential reflectograms could be reproduced by taking the derivative of a quantum mechanical expression for the reflectivity

with respect to alloy composition. This treatment confirms our assumption that the structure in the differential reflectograms is indeed caused by electron transitions.

It was found that the threshold energy for d-band to Fermi energy transitions does not change for alloy compositions up to approximately 1 at.-% solute concentration, thus confirming the theory by Friedel involving screening of solute charges at low alloy concentrations. The experiments further indicated that the Fermi energy is raised much less due to solute additions than predicted by the rigid band model and that the d-bands are possibly raised by alloying.

A behavior similar to that involving transitions from the top of the d-bands to the Fermi energy was found for the shift of a transition around 5 electron volts. This confirms theoretical considerations that at this energy, transitions from the lower d-bands to the Fermi energy are involved. The larger shift of this 5 electron volt peak with increasing solute concentration compared to the threshold energy seems to indicate that the lower d-bands are not affected as much as the upper d-bands by alloying.

A further transition around 4 electron volts behaves in many respects differently than the before mentioned transitions and is observed to decrease in energy with increasing solute concentration. Conduction band to Conduction band transitions are believed to be involved in this structure.

Copper-Gold alloys do not show any change in the threshold energy due to solute additions, thus indicating that the Fermi energy as well as the copper d-bands remain unchanged with alloying. Additional structure between 2 and 5 electron volts indicate that transitions from the Gold d-bands may be involved.

CHAPTER I
INTRODUCTION

The optical constants of pure metals have been systematically measured by Drude and others as far back as the end of the last century. Since then, there have been attempts to increase the accuracy of these measurements for the purpose of obtaining the material constants as well as for comparing the optical data with the electron theory of metals. From early findings it was clear that Drude's free electron theory was adequate in the infrared, but failed to reproduce the experiments for some metals in part of the visible and the ultraviolet frequency range. With the discovery of quantum theory, it was recognized that optical absorption in these frequency ranges was due to transitions of electrons from filled energy states or "bands" to higher, unfilled energy states (interband transitions). Attempts were made to separate the free (i.e. Drude-type) electron part in the spectral reflectivity from the effect of interband transitions, with the ultimate goal of identifying the photon energies at which "structure" was observed.

At approximately the same time that these developments were in progress, detailed theoretical band calculations for the pure metals were being made available. The observed structure in the spectral optical behavior which might be the result of interband transitions could then be identified with the help of these calculations. On the other hand, the experimental work provided a useful means of checking the calculated band structure by providing the "gap energies."

One may ask: Why the great interest in the optical properties of materials? These experimentally determined parameters give much information as to the electronic structure and properties of a material. The electronic structure of a material determines many of its important technological properties, for instance, electrical and thermal conductivity, ordering, alloying, or bonding. A long range objective is that even mechanical or other properties of materials will be understood on the basis of their electronic structure.

The classical technique for determining the reflectivity of a metal is to shine light of a particular wavelength on it and measure the incoming intensity and the amount of light which is reflected from its surface. A typical curve of reflectivity versus wavelength of light is shown in Figure 1.1. As an example, pure copper is chosen. It can be seen that this curve shows some defi-

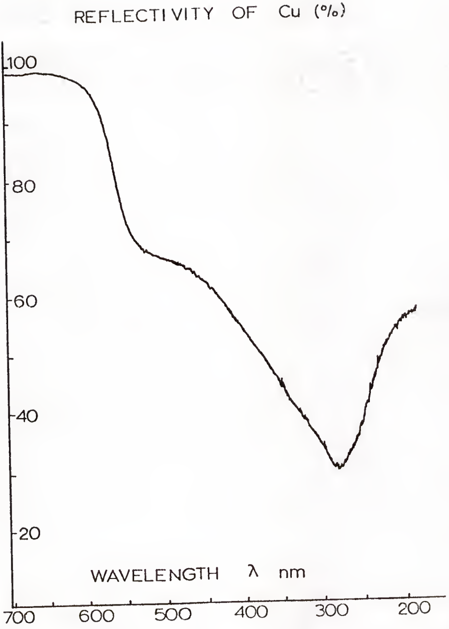

Figure 1.1. The reflectivity of copper in the wavelength range of 700 nm to 200 nm

nite discontinuities (called "structure"), but that these features are not sharp or well pronounced. The observed changes in reflectivity are known to be due to absorption processes in the metal, that is, electrons from a low energy state are absorbing energy from the incoming radiation and are being lifted to a higher energy level. However, the exact energy at which this transition in the electronic structure of the metal is taking place is difficult to determine from the reflectivity spectrum due to the broadness of the structure. This broadness is due to the interactions of electrons and atoms in a crystal. (In contrast to this, the optical spectra of gases are providing the well-known, "sharp" absorption lines.)

The interpretation of the optical structure of solids is nontrivial. The reason for that is that they could be caused by a summation of a variety of possible transitions. For example, the energy for a given absorption peak in copper may be taken from Figure 1.1 to be 4.8 ev. If one shines monochromatic light of that energy onto copper, it could cause all possible transitions for which the occupied, initial states and the unoccupied, final states are separated by 4.8 ev. The band structure diagram for copper, however, provides only certain high symmetry directions in k space. Nevertheless, it is necessary to consider transitions at all points in the Brillouin zone as far as they are not forbidden by selection rules. These considerations make it clear that disentangling the optical structure is not easy. Fortunately, it is also not completely hopeless. It is widely assumed that certain transitions, especially those near symmetry points, are sometimes sufficiently strong that they show up quite clearly and can be readily interpreted.

With the recent onset of modulation techniques, which enhance the structure in the reflectivity of metals or semiconductors, new interest has arisen concerning the use of optical techniques for the determination of the electronic structure of materials. Modulation spectroscopy includes various experimental techniques in which the optical properties of a material are measured as an oscillating pertubation, which modulates the band structure of the material, is applied to it. The optical property measured may be the amount of transmitted or reflected light. By observing the change in properties, essentially the derivative with respect to the pertubation is obtained.

The modulation technique used in the present investigations involved a modulation of the composition between two alloys within the same binary alloy system. It will be shown that this technique is a valuable tool of precisely locating major transitions in the interband absorption of solids.

Much work has been done on determining the electronic structure of pure metal crystals, that is, band calculations have been made and many different types of experimental techniques have been applied to them in order to determine the transition energies and correlate them with the theoretical work. However, the theory of alloys is still rather primitive. Solid solution alloys represent mostly a disordered system for which it is difficult to formulate a theoretical model. The main problem appears to be the lack of a means of modeling the potential at each lattice site in the disordered structure. Interest, however, in the alloy systems has greatly increased within the past few years. It is known that the addition of an alloying element to a metal, as a rule, changes its band structure. Just how this band structure changes and the effect on the optical transitions with changing composition has opened up a whole new area of interest both from an experimental and a theoretical aspect.

The purpose of the work which will be reported here was to make a quantitative experimental investigation of the change in the electronic structure of copper upon the addition of various amounts of impurities to it. The following table represents the elements which were alloyed with copper. All alloys were within the α solid solution region of their respective phase diagram. The changes in energies for several interband transitions of copper with alloying were observed. An attempt will be made to correlate the experimental results with existing theoretical models.

In the following chapter, a discussion of the existing literature on the optical and electronic properties of copper and some of its alloys will be given. In Chapter III, the experimental procedure used in the current investigations will be outlined. Chapter IV will present the theory necessary to understand the connections between the optical properties of a material and its electronic structure. This chapter will also include the theory behind the technique of compositional modulation. In Chapter V, the results obtained on the various α phase copper alloys studied will be presented. The final chapter, Chapter VI, is a discussion of the results presented in this study by employing existing theories of the band structure of alloys and conclusions will be drawn as to the effect of increasing solute concentration of the different metals.

Table 1.1

Elements Which Were Alloyed With Copper
Au
Zn
Al
Ga
Ge
Si
Sn
As

CHAPTER II
LITERATURE SURVEY

II-1 General Remarks

The optical constants of pure noble metals have been studied in great detail, and within the past ten years, this work has been supplemented to an increasing extent on noble metal alloys. Unfortunately, a variety of techniques have been used for the different alloy systems and this makes it rather difficult to make reliable comparisons between them. Likewise, the existence of considerable disagreement between various band calculations, alloy theories, and experiments regarding the number and location of the interband transitions in copper has been of concern for some time.

In an effort to illuminate the present situation, this section will review the literature concerning the theoretical models governing interband transitions in copper and its alloys, and try to correlate the theory with experimentally determined values. There appears to be, as will be seen, a lack of agreement between authors in the field.

As far back as 1936, Mott and Jones[1] postulated that the main absorption edge observed in the spectral reflectivity of copper was due to electron transitions from the d-bands of the crystal to unoccupied states immediately above the Fermi energy. Hence, it was supposed that on alloying, the shift in the absorption edge to higher energies should be equal to the displacement of the Fermi level. It was assumed that there is very little change in the relatively low lying d-bands. This theory, which is known as the "Rigid Band Model" (RBM), postulates that the alloy has essentially the same electronic structure as the pure host but with a Fermi energy determined by the type of solute metal addition. The effect of adding solute metal atoms, whose valency is higher than that of the solvent, is to fill the density of states curve and thus raise the Fermi energy to a higher level. Hence, a shift in the absorption edge to higher energies should be observed upon alloying.

Friedel[2] proposed a modification to the Mott theory, taking into account screening effects. That is, the excess charge donated by the impurity localizes around the impurity atom and does therefore not contribute to the "sea" of electrons. According to this view, for a low concentration of impurities, the absorption edge should not differ from that in pure copper. Therefore, alloying should not cause any appreciable shift in the optical absorption edge, apart from relatively small effects due to changes in coulomb attraction between the screening charges and the lattice.

As a result of the broadness of the absorption edges, the restricted frequency ranges covered, and the small number of alloys studied, the older work was incapable of distinguishing between these theories in a satisfactory way, or of providing useful information about the band structure of noble metal alloys in general. Since this older work, much more reliable optical measurements have been made on copper and copper alloys and new theories have been developed to explain the results. This new wave of interest began in the early '60s and has continued up to the present time.

One of the first experimental pieces of work was done in 1959 by Biondi and Rayne[3] who measured the optical absorption of brasses using a calorimetric method (see Figure 2.1). They observed the main absorption edge in copper at 2.15 ev, and assigned this to a d-band to Fermi energy transition. They noticed that as the Zn concentration increased, the edge moved to higher energies. The displacement of the edge was initially quite small and later became larger and linear beyond 3 at.% Zn. In light of their results, they concluded that the shift of the

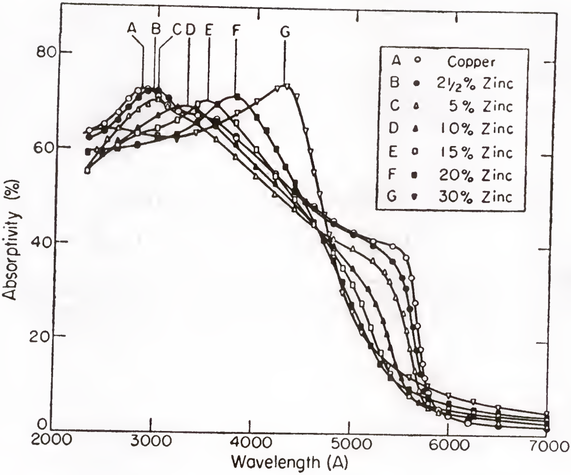

Figure 2.1. Optical Absorptivity of α-brasses in the ultraviolet and visible regions (from Ref. 3)

edge on alloying was inconsistent with the original theory of Mott. Although the Friedel theory gave a better fit to the experiment, there was still a qualitative disagreement regarding the dependence of the shift on solute concentration.

II-2 Pure Copper

Around 1962, a detailed band calculation for copper became available.[4] This diagram is shown in Figure 2.2. The observed features in the spectral reflectivity or absorptivity which resulted from interband transitions could now be related to this diagram. A re-examination of the available experimental optical data of copper was undertaken by Ehrenreich and Philipp[5] using this band diagram. They plotted the experimental absorption coefficient for copper (which they obtained by a Kramers-Kronig Analysis from reflectivity data) over the spectral range 1 - 25 ev (Figure 2.3), and tried to correlate the photon energies where structure was observed to certain transitions in the band structure. They associated an absorption at approximately 2.1 ev with a transition of electrons from a d state to the Fermi energy, in particular the transition $L_3 - L_{2'}(E_F)$. Similarly, they associated the observed structure around 5 ev with the $X_5 - X_{4'}$ and the $L_{2'} - L_1$ transitions.

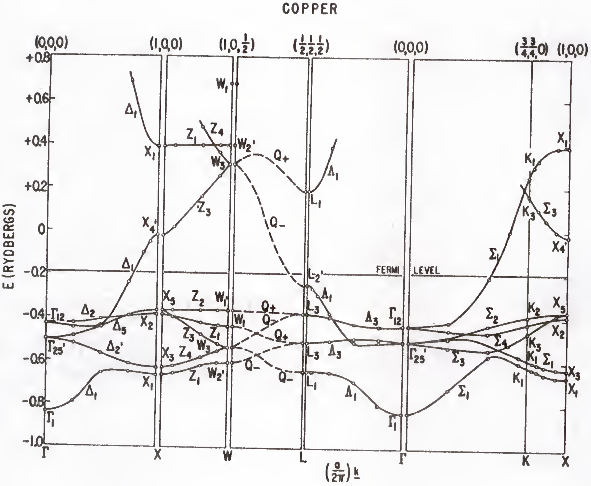

Figure 2.2. Energy Band Diagram of Copper (from Ref. 4)

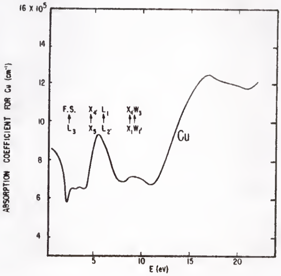

Figure 2.3. Spectral Dependence of the absorption coefficient of Cu over the range 1 → 25 ev (from Ref. 5)

Another technique, photoemission spectroscopy, was applied to copper by Berglund and Spicer[6] in 1964 in an attempt to interpret the energies of photoemitted electrons in terms of the band structure of copper. From their results, it was concluded that strong transitions were likely near $X_{4'}$ and $L_{2'}$ which correspond to peaks in the density of states curve.

Later on, Spicer[7] followed up his previous work with additional photoemission experiments and from these made some general conclusions about the probability of direct and indirect transitions in copper. He felt that k conservation is important for transitions from s and p like states, but is less likely for transitions from d like states.

Cooper, Ehrenreich and Philipp[8] (1965) extended the work done previously by Ehrenreich and Philipps by examining the low energy structure in the reflectivity of copper by means of absolute calculations of the imaginary part of the dielectric constant. They showed that in the case of metals, sharp optical structure may also arise from transitions between relatively flat d-bands, such as, for example, the upper d-band, and empty states just above the Fermi surface, in addition to those at critical points. In light of the statements of Berglund and Spicer,[6] Cooper et al.[8] used the insight they obtained from their calculations to examine to what degree the direct processes explain the observed results. They stressed that while it is valuable to correlate the photoemission results with ordinary optical absorption, photoemission is a more complicated process since in addition to the photon absorption, it involves the processes of electron escape from the solid to the vacuum. It is not clear to what extent, if any, this complication obscures identification of initial excitation processes. They concluded that while photoemission work suggests that indirect transitions may appear to contribute to the optical structure for the noble metals, there is no other clear experimental evidence indicating that they are a dominant factor describing the interband optical properties.

Speculations on the theoretical implications of the dielectric constant of copper was also given by Beaglehole (1966).[9] He tried to relate structure in the optical absorption spectra of copper below 10 ev to the band structure calculated by Segall.[4] In trying to assign these peaks to particular interband transitions, he finally concluded that an unambiguous assignment was not possible at this time. His major criticism of the work done by other authors was that they ignored transitions from the lower d-bands, presumably on the grounds that at the symmetry points X and L, such transitions were forbidden. Beaglehole felt that indeed the peak observed in copper at 2.5 ev is due to a d-band to Fermi level transition but that the observed peak around 3.5 ev and part of the peak at 5.5 ev could be due to excitations from lower d-bands to states in the neighborhood of L. He also speculated that at about 5 ev in copper, it should become possible to excite valence electrons from occupied states near L into band 7.

Piezo-optical measurements have also been used to identify electronic transitions in metals. In this technique, a uniaxial strain induced change in reflectance is used to determine the change in ε_2. By applying a uniaxial stress in certain directions, it is possible to distinguish between singularities of different symmetry. Gerhardt, Beaglehole, and Sandrock (1967)[10] observed structure in $\Delta\varepsilon_2$ at 3.9 ev which they attributed to what they felt was the only possible transition, that is, $X_5 - X_{4'}$. They also observed a peak around 4.3 ev which they attributed to the $L_{2'} - L_1$ transition. They agreed with other authors that the transition around 2 ev is from the top of the d-bands to the Fermi energy, which is probably near L.

Gerhardt[11] studied the response of the optical constants of copper to a strain in the range 1.5 - 5.5 ev. He assigned the transition at 4.0 ev to $X_5 - X_{4'}$, and the transition at 4.15 ev to $E_F - L_1{}^u$. The 2.1 ev edge was shown to start at Q near L, but at slightly higher energies, various parts of the Brillouin zone were believed to contribute. His measurements were consistent with the assumption that direct interband transitions dominate the absorption above 2 ev.

New theoretical input was given by Mueller and Phillips[12] (1969), who used the random phase approximation method to calculate the optical spectrum of copper. They compared their calculated spectrum for ε_2 with available experimental data (Figure 2.4). They assign the first experimentally observed peak at 2.1 ev to the d-band E_F transition near X and the second observed edge at 2.9 ev to the d-band - E_F transition near L. It is interesting to note that they concluded from their calculations that the peak observed around 4.8 ev arises not from $X_5 - X_{4'}$, but from $L_{2'} - L_1$. (These transitions are called by Mueller and Phillips conduction band to conduction band transitions.) The $X_5 - X_{4'}$ transition showed only a weak structure in their calculated ε_2 curves. The observed peak slightly greater than 5 ev was attributed to transitions from the lower d-bands ($L_1{}^\ell$) to $L_{2'}$ at E_F.

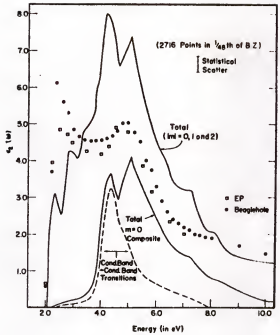

Figure 2.4. Plot of interband contribution to $\varepsilon_2(\omega)$ in the range $1.5 \leq \hbar\omega \leq 10$ ev for Cu (from Ref. 12)

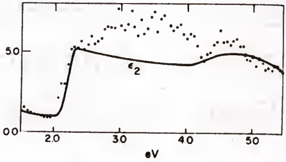

Figure 2.5. Energy dependence of ε_2 for Cu (from Ref. 13)

Dresselhaus[13] (1969) also calculated the theoretical curve for ε_2 vs. energy for copper (Figure 2.5) and by comparing it to experimental data, assigned the transition at 2.2 ev to d-band → E_F transitions and structure at 4.2 ev to transitions from the lower d-bands to E_F.

II-3 Copper Based Alloys

Around the early 60's, interest was aroused into the investigation of the optical properties of alloys. Some work has been done on the optical spectra of alloys consisting of noble metals to determine the interaction between the d-bands of the two constituents. Work was also done on the noble metal alloys containing transition metals such as Cu-Pd and Cu-Mn. These works were primarily concerned with the investigation of virtual bound states on the solute atoms.

Pant and Joshi[14] used a theoretical model, the coherent potential approximation, to describe the electronic spectrum of Cu-Zn alloys. They compared their results to the experimental data of Biondi and Rayne and concluded that their theory disagreed with the experimental data. Table 2.1 shows a comparison of experimental and theoretical results for changes in transition energy from copper to Cu-30 at.% Zn.

Table 2.1

Experimental and Theoretical Results for Changes in transition Energy from Copper to Cu-30 at. Zn (from Ref. 14)

Transition	$(L_1 \rightarrow L_{2'})$	$(X_5 \rightarrow X_{4'})$	$(E_F \rightarrow L_3)$
Experimental			
Biondi & Rayne	0.096		0.026
Theoretical			
ATS	0.094	0.008	0.035
Avg t matrix	0.013		0.062
Pant & Joshi	0.021	0.021	0.005

Lettington[15] also analyzed the experimental data of Biondi and Rayne.[3] He concluded that with increasing Zn concentration, the absorption edge at 2.2 ev of pure copper moves to higher energies, while the peak initially at 4.2 ev moves to lower energies. A comparison of Biondi and Rayne's and Leetington's peak assignments are listed in Table 2.2.

Table 2.2

Comparison of Peak Assignments of Cu-Zn Alloys (from Ref. 15)

Author	2.2 ev	3.45 ev	4.3 ev
Biondi & Rayne	$L_3 \rightarrow L_{2'}(E_F)$		$L_{2'} \rightarrow L_1$
Lettington	$L_3 \rightarrow L_{2'}(E_F)$	$L_{2'} \rightarrow L_1$	$X_5 \rightarrow X_{4'}$

Lettington monitored the change in the transition energies for various alloys of increasing Zn concentration. From these results, he concluded that:

1. with increasing Zn concentration, the difference between the top of the d-bands and the Fermi energy is slightly increased.
2. the top of the conduction band at $X_{4'}$ moves down with respect to X_5 upon alloying.

Lettington concluded that, due to screening effects, the actual movement of the band edge was much less than that predicted by the rigid band model. He therefore modified this model by postulating that the d states of copper may be changing upon alloying.

Amar, Johnson, and Sommers[16] (1967) calculated the band structure of alpha brass (αCuZn) as a function of composition from 0% Zn up to 30 at% Zn. One of the assumptions made in their calculations was that the Cu d-bands are unchanged by alloying. Figure 2.6 shows their findings. The solid lines denote the band structure of pure copper and the dotted lines refer to the band structure of Cu-30% Zn. As can be seen, the main effect of alloying is a general displacement of the conduction bands to lower energies. Γ_1, $X_{4'}$, $L_{1'}$ and $L_{2'}$ levels also decrease in energy with alloying. The decrease in $L_{1'}$ is

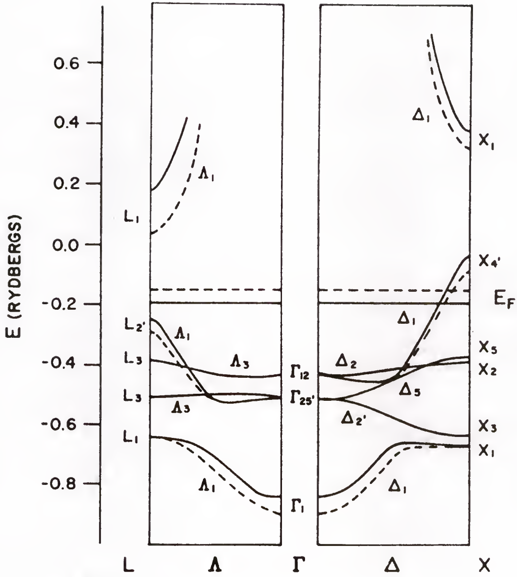

Figure 2.6. Comparison of energy bands of copper (solid lines) with those of Cu-30at.% Zn (dashed lines) (from Ref. 16)

somewhat larger though, resulting in a reduced $L_{2'} - L_1$ energy gap with alloying.

Pells amd Montgomery[17] (1970) studied systematically the optical properties of various α phase copper alloys to test the theories of alloy structure using a uniform procedure for all the alloy systems investigated. They measured the absorption spectra of bulk copper alloys from 1.7 - 5.9 ev using polarimetric techniques in a high vacuum. Their main concern was the exact identification of the photon energies at which various structures of the spectra occur.

For all alloys, the absorption observed near 2 ev was broadened and shifted to higher energies as the solute concentration increased. The new contribution made by these authors was the observation that a single peak occurring in the absorption curve of pure copper around 5 ev was apparently splitting into two sub-peaks in the alloys, which they refer to as the high and low energy peaks (Figure 2.7a, b, c, d). In Cu-Ga, the two peaks were shown to have the same intensity, whereas in the Cu-Zn, the low energy peak was more pronounced, in Cu-Ge the high energy peak was more pronounced, and in Cu-As only the high energy peak was found to be visible. This 5 ev peak was interpreted to be composed of absorptions at

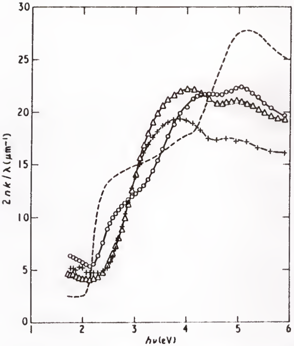

Figure 2.7a. Cu-Zn absorption spectrum at 295°K. Broken curve, pure copper; O Cu-Zn 16at.%; Δ Cu-Zn 27at.%; + Cu-Zn 32at.% (from Ref. 17)

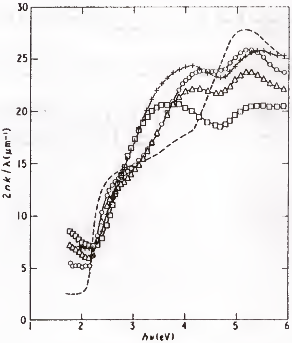

Figure 2.7b. Cu-Ga absorption spectrum at 295°K. Broken curve, pure copper; O Cu-Ga 6at.%; Δ Cu-Ga 8at.%; + Cu-Ga 12at.%; □ Cu-Ga 16at.% (from Ref. 17)

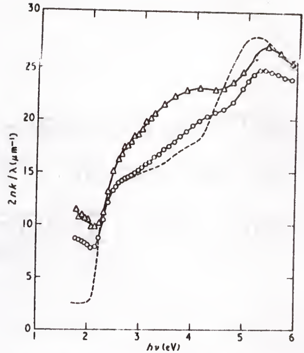

Figure 2.7c. Cu-Ge absorption spectrum at 295°K. Broken curve, pure copper; O Cu-Ge 4at.%; Δ Cu-Ge 8at.% (from Ref. 17)

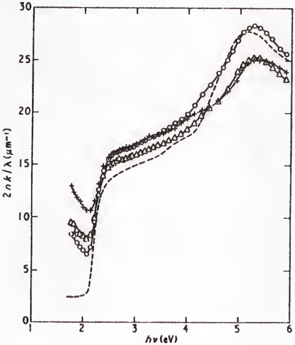

Figure 2.7d. Cu-As absorption spectrum at 295°K. Broken curve, pure copper; O Cu-As 2at.%; Δ Cu-As 4at.%; + Cu-As 6.5at.% (from Ref. 17)

4.8 and 5.4 ev. With increasing amounts of solute, the 5.4 ev peak remained relatively stationary, whereas the 4.8 ev peak decreased in energy. They assigned their low energy peak to the $L_{2'} - L_1{}^u$ transition and their high energy peak to the $L_1^\ell - E_F$ transition. In making these assignments, they weighed the evidence of previous authors.

In carefully looking at Figure 2.7a, b, c, d, a different interpretation can be arrived at. A small amount of structure can be seen in the pure copper curve at the energy of the low energy peak (approximately 4.2 ev). If Pells and Montgomery would have presented data for lower alloy compositions, a more conclusive assignment of their data could be given. Differential reflectometry, which enhances the structure in the spectral reflectivity, is capable of shedding some light on this question. In Table 2.3, the basic assignments made up to the time of their work is shown.

Pells and Montgomery's work was in general agreement with the more limited data obtained by Biondi and Rayne.[3] However, due to the work by Mueller and Philipps,[12] who found that the $X_5 - X_{4'}$ transition contributes very little to the structure of the optical absorption of copper, Pells and Montgomery ruled out this transition. In specu-

Table 2.3

Assignments of Structure in the Optical Spectra of Cu and Cu Alloys

Investigator	Kind of Work	Transition	Energy
Biondi & Rayne	exp	$d \rightarrow E_F$	2 ev
Lettington	th	$d \rightarrow E_F$	2.2 ev
		$L_{2'} \rightarrow L_1^u$	3.45 ev
		$X_5 \rightarrow X_{4'}$	4.3 ev
Mueller & Philipps	th	$L_{2'} \rightarrow L^u$	4.8 ev
		no X-transition	
Gerhardt	exp	$X_5 \rightarrow X_{4'}$	4.0 ev
		$E_F \rightarrow L_1^u$	4.15 ev
Pells & Montgomery	exp	$d \rightarrow E_F$	2.2 ev
		$L_{2'} \rightarrow L_1^u$	4.8 ev
		$L_1^\ell \rightarrow E_F$	5.4 ev

lating on the probable effects of alloying on the band structure of copper, in relation to their experimental data, they felt that when a polyvalent solute is dissolved in copper the conduction bands are common to both constituents and are only depressed in energy relative to pure copper. The results were interpreted in such a way that the Fermi energy rises in the alloys, but much less rapidly than it would be expected based on the rigid band model. However, the d states of the solute atoms were believed to lie far below those of the solvent and can be ignored. These authors made an interesting assumption that upon alloying, a narrowing of the d-bands would occur due to the dilution by the solute atoms. With this in mind, an implication was made that possibly the top of the d-bands were decreasing in energy, while the bottom was increasing. Applying this to their optical data, they concluded that upon alloying, the d-bands and the Fermi energy should move apart, as was observed by the increase in the energy of the 2.2 ev transition due to alloying. The situation for the L_1^{ℓ} - E_F was less convincing because both these levels should rise with alloying. The fact that the high energy peak remains apparently the same suggests that $L_1{}^{\ell}$ and E_F are raised by similar amounts. Bands $L_{2'}$ and $L_1{}^{u}$ both are supposed to move down in energy, $L_1{}^{u}$ moving down more due to the dilution of the Cu d-bands. Therefore, the movement to lower energies of the low energy peak is observed.

Soven[18] used an "average t-matrix model" calculation to determine the behavior of the d-bands in Cu-Zn alloys. He acknowledged the fact that the d-bands may be moving.

He also calculated the changes of the band gaps as a function of composition and when he compared these to the experimental data, a discrepancy was found. Soven rationalized the difference by suggesting that his assumption of direct transitions may be wrong.

II-4 Recent Results Using Modulation Techniques

Around 1965, optical derivative spectroscopy was developed, and modulation techniques began to be widely used in order to more clearly determine the optical transitions occurring in metals. Fong et al.[19] (1970) applied wavelength modulation spectroscopy to metals at low temperatures (Figure 2.8). (In wavelength modulation, an up-down type structure corresponds to one transition.) The origin of most of the structure in the measured derivative spectrum of copper was determined using the theoretical band structure of copper, calculated by Fong et al. using the "empirical pseudopotential method." In examining their data, they tried to identify some of the important interband transitions in copper. Their results are summarized in Table 2.4. They also calculated ε_2 as a function of energy using pseudo wave functions and then from these values calculated a derivative curve (wavelength modulation curve) (Figure 2.8). The general struc-

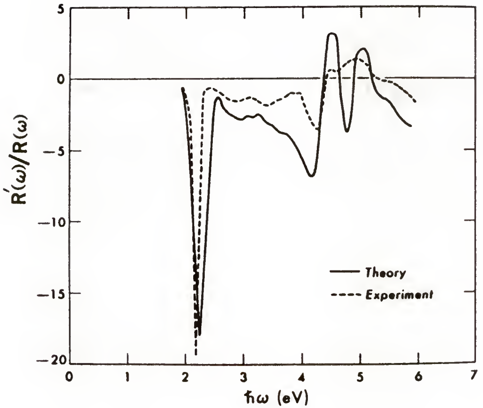

Figure 2.8. Experimental and calculated wavelength modulation curves for copper at T = 7°K (from Ref. 19)

Table 2.4

Identification of the Important
Interband Transitions of Cu (from Ref. 19)

Transition	Energy	Symmetry
$\Delta_5 \rightarrow \Delta_1$ (5 → 6, 4 → 6) 5th d → E_F	2.1 ev	osculating point
Large (5 - 6) (4 → 6) inside BZ near X and E_F	3.2 ev	volume effect
$\Sigma_1 \rightarrow \Sigma_1$ (3 - 6)	3.7 ev	osculating point
Large (5 → 6) (4 → 6) (3 → 6) inside BZ near X and E_F	3.7 ev	volume effect
$X_5 \rightarrow X_{4'}$ (4 → 6) (5 → 6)	3.96 ev	critical point
$L_{2'} \rightarrow L_1^u$ (6 → 7)	4.25 ev	critical point
$\Sigma_1 \rightarrow \Sigma_1$ (1 → 6)	4.38 ev	osculating point
Large (5 - 6) (4 → 6) (3 → 6) inside BZ near E_F	4.5 ev	volume effect
Large (2 → 6) (1 → 6) inside BZ near E_F	5.0 ev	volume effect

ture of the calculated and the experimental derivative curves agree very well. The interband transitions start at 2.1 ev. The calculated derivative curve shows some structure at 3.7 ev, while the measured curve has a twin peak structure at 3.8 and 3.95 ev. The influence of the critical point at 3.96 ev from the X_5 - $X_{4'}$ transition does not show up clearly in the calculated derivative curve, but can be seen in the calculated ε_2. They associated this transition with the upper structure of the twin peaks in the experimental curves. Their results strongly support the findings of Mueller and Phillips[12] that the 5 ev peak in ε_2 consists of a threshold at 4.3 ev stemming from $L_{2'}$ - $L_1{}^u$ and a shoulder at 4.8 ev corresponding to d-band - E_F transitions.

The main conclusions which they arrive at by comparing their theoretical and experimental derivative curves with ε_2 are:

1. The optical transitions in copper are direct.
2. The observation of the X_5 - $X_{4'}$ transition agrees with the suggestions of Mueller and Phillips[12] who stated that this transition can be seen in the calculated ε_2 only very weakly.
3. The composite nature of the 5 ev peak agrees

with suggestions by Mueller and Phillips.[12] However, Fong *et al.*[19] assign the upper structure to volume effects.

Welkowsky and Braunstein[20] (1971) followed up this previous work by also applying wavelength modulation to copper in the range 2 - 5 ev. They then transformed their derivative data by use of a Kramers-Kronig analysis to yield an ε_2 vs. energy spectrum. In their derivative curve (derivative of reflectivity with respect to energy, shown in Figure 2.9), they observed a shoulder at 2.18 ev, which they attributed as usual to d-bands → Fermi surface transitions, specifically to $\Delta_5 - \Delta_1(E_F)$ and $L_3(Q+) - E_F(L_{2'})$. The first peak in ε_2 (Figure 2.10) was seen at 2.53 ev and was interpreted to correspond to the transition $L_3(Q_-) - E_F(L_{2'})$. (It is interesting to note that these authors, through their peculiarity in arriving at ε_2, obtained a peak in ε_2 at this energy, where other authors do normally not observe pronounced structure.) The second peak at 3.75 ev was associated with the transition $X_5 - X_{4'}$, and the third peak at 4.74 ev was assigned to the conduction band transition $L_{2'} - L_1$. A very weak structure at 3.26 ev was also observed and was attributed to volume effects near X and L. Their results, supported with the symmetry results of Gerhardt,[11] were believed to "conclusively different-

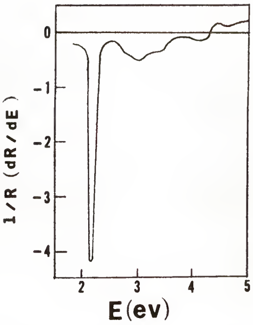

Figure 2.9. Derivative of Reflectivity with respect to energy of Cu at 80°K (from Ref. 20)

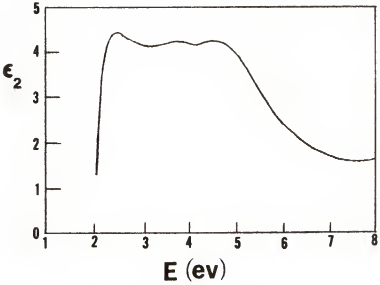

Figure 2.10. Imaginary part of the dielectric constant, ε_2, for Cu obtained at 80°K by a Kramers-Kronig analysis (from Ref. 20)

iate" between the X and L transitions. (This statement, however, does not appear to be substantiated by their results.)

Williams, Janak, and Moruzzi[21] (1972) calculated the interband absorption $\varepsilon_{2ib}(\omega)$ and the energy distribution of photoemitted electrons for copper in order to determine the magnitude of the L gap. They attribute their initial structure in ε_{2ib} to transitions involving d-states and conclude that the $L_{2'} - L_1$ transition occurs at 4.2 ev.

The optical constants n and k were obtained for copper by Johnson and Christy[22] (1972) from reflection and transmission measurements on thin films at room temperature in the range 0.5 - 6.5 ev. ε_2 values as a function of wavelength were then calculated from the data. Figure 2.11 shows their experimental ε_2 spectrum compared with the theoretical curves of Williams _et al._[21] and Fong _et al._[19] They observe two pronounced peaks, one near 2.5 ev and another near 5 ev, along with some other fine structure. Their experimental values lie between the two theoretical curves, but somewhat closer to Fong's results. Both theoretical curves exhibit the same general structure as the experimental curve. The slight shoulder observed near 4.5 ev is seen in the calculated curve of Williams

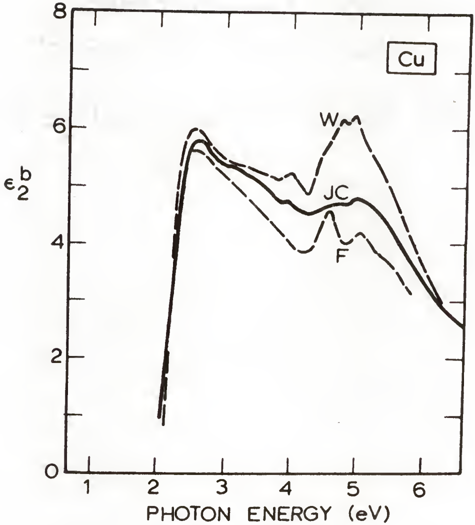

Figure 2.11. Experimental values of ε_2 for copper as a function of photon energy. Also included are the theoretical curves of Williams et al.[21] and Fong et al.[19] (from Ref. 22)

et al. However, the authors feel that Fong et al. overestimated its size. Johnson and Christy's experimental data also showed a small peak near 4 ev, which can be identified in the theoretical curve of Williams, but not in the one by Fong.

Using the "single site coherent potential approximation," Das and Joshi[23] calculated a band diagram for Cu-30 at.% Zn. The peaks in pure copper at 2.2 ev and 3.45 ev were observed to increase in energy upon alloying and the peak at 4.8 ev decreased upon alloying. By calculating the spectral density of states in α brass, they assigned the following transitions to respective energies:

2.2 ev	$L_3 - L_{2'}(E_F)$
3.45 ev	$X_5 - X_{4'}$
4.3 ev	$L_{2'} - L_1$

It should be noted here that their assignments for the second and third peaks in copper are exactly opposite to those of Lettington.

Work, done by Hummel and Andrews,[24] starting in 1960, on several α phase copper alloys using compositional modulation showed three pronounced peaks. (This technique is capable of detecting changes in the band structure due to alloying.) They associated their peaks with the d-band → E_F transition around Δ and to $X_5 - X_{4'}$, and $L_{2'} - L_1$

transitions. The first transition was found to increase, while the other two decreased in energy with increasing solute concentration. They further found that the shift of the threshold energy for interband absorption was increasing much slower with solute concentration than predicted by the rigid band model and attributed this to possible raises of the d-bands due to alloying.

DeReggi and Rea[25,26] measured the reflectivity of various Cu-Al, Cu-Ga, Cu-Ge, Cu-Zn, and Cu-As alloys with conventional methods. They speculated on the possibility of indirect transitions in these alloys. Their main observations derived from their ε_2 curves (Figure 2.12) (obtained by a Kramers-Kronig analysis of the reflectivity data) were

1. a threshold at 2.2 ev due to d-band → E_F transitions which increases in energy upon alloying.
2. a peak at 4.3 ev which is assigned to interconduction band transitions (ICB) $L_{2'}(E_F) - L_1$ (Figure 2.13), which decreases in energy upon alloying.
3. a peak at 5 ev which corresponds to transitions from low lying d-bands to states at E_F. This transition also decreases in energy upon alloying.

DeReggi and Rea speculated that at low alloy concentra-

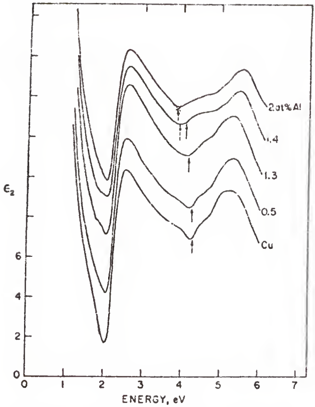

Figure 2.12. Imaginary part of the dielectric function (ε_2) for Cu and for low concentration Cu-Al alloys at room temperature (from Ref. 25, 26)

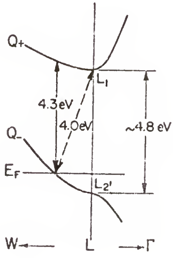

Figure 2.13. Energy bands of copper near the L symmetry point, showing the direct neck gap (4.3 ev), and the indirect neck gap (4.0 ev) (from Ref. 25, 26)

tions, the ICB transition is direct and decrease from 4.3 ev to 4.0 ev with alloying. At solute concentrations larger than about 2%, indirect transitions were believed to be present. The exact composition of the alloy where indirect transitions began is dependent on the solute type, but was usually between 2 and 3% solute. The indirect neck gap was also assumed to decrease in energy as the solute concentration increases. This effect is shown in Figure 2.14. Their explanation involves a "sinking conduction band," that is, upon alloying, band L_1^u drops in energy fairly linearly (about 0.1 ev/at% Al) as the concentration of solute increases.

Rosei and Lynch[27] (1972) applied thermomodulation (a method where the temperature of the sample is periodically changed during measurement) to thin film samples. They measured thermoreflectance and thermotransmission and calculated from that $\Delta\ \varepsilon_2$ directly without a Kramers-Kronig analysis. They compared their results with piezomodulation measurements and tried to resolve some of the discrepancies in the interpretation of the optical properties of copper. The most striking features in their thermotransmission, thermoreflectance and $\Delta\ \varepsilon_2$ spectrum were (see Figures 2.15 and 2.16)

1. a sharp derivative peak at about 2.15 ev.

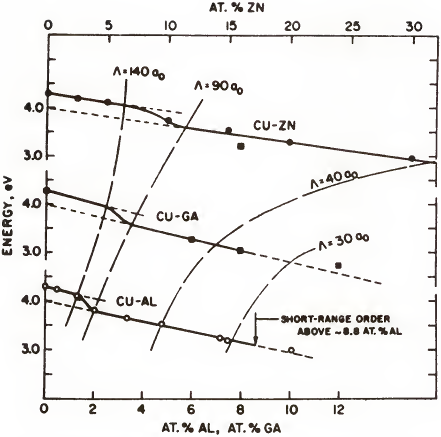

Figure 2.14. Energy location of the observed onset of interconduction-band absorption as a function of solute concentration. Direct neck gap at low concentrations and indirect neck gap at high concentrations. (from Ref. 26)

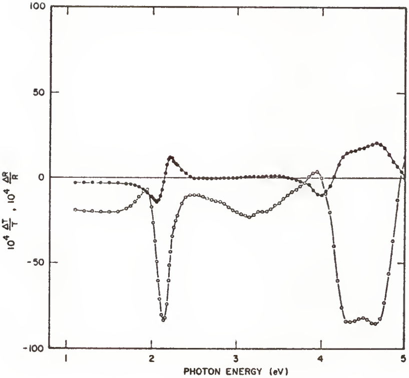

Figure 2.15. Thermotransmission and thermoreflection spectra of a 455 Å thick film of copper at 350°K. Open circles represent ΔT/T and closed circles ΔR/R (from Ref. 27)

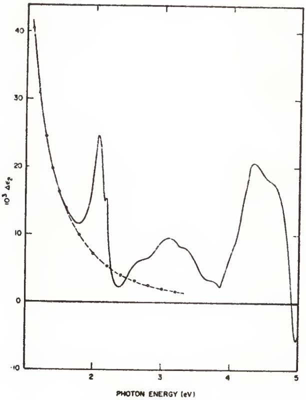

Figure 2.16. $\Delta\varepsilon_2$ spectrum resulting from spectra in Figure 2.15 (from Ref. 27)

2. a rather broad structure in the range 2.4 - 3.6 ev, with a shoulder at 3.2 ev.
3. a small structure at 4 ev.
4. a strong twin peak at 4.3 and 4.8 ev.

The structure at 2.15 ev was assigned to the $L_3 \rightarrow E_F$ transition. Their modulation spectrum shows very similar structure and the same critical energies as Fong *et al.* reported for wavelength modulation. They assigned the shoulder at 4 ev to the $X_5 - X_{4'}$ transition, while the 4.8 ev structure was believed to be due to transitions from lower lying d-bands to the Fermi surface.

Beaglehole and Erlbach[28] (1972) studied dilute noble metal-noble metal alloys. They used a similar but somewhat different method as utilized in the present work. They compared the reflectance of all alloys with that of the pure metal and effectively measured a quantity proportional to the difference in reflectance. In their spectra of Cu-Au alloys (see Figure 2.17), they assigned the following transitions to electron energies:

2.1 ev	$d \rightarrow E_F$
3.9 ev	$X_5 \rightarrow X_{4'}$
4.1 ev	$E_F \rightarrow L_1^u$
4.3 ev	$L_{2'} \rightarrow L_1$
4.8 ev	$L_1^{\ell} \rightarrow E_F$

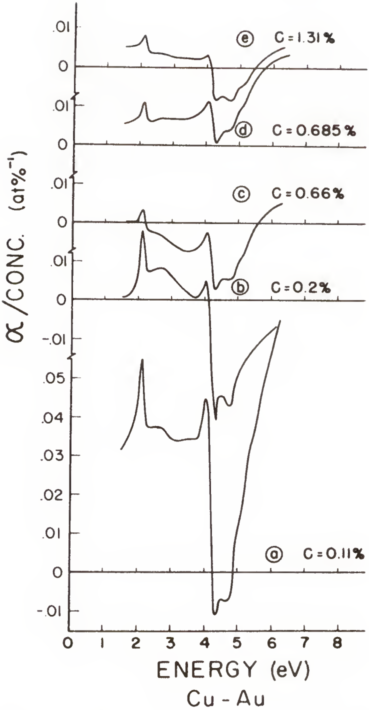

Figure 2.17. Experimental curves of α/c where $\alpha = \frac{(R_{pure} - R_{alloy})}{(R_{pure} + R_{alloy})}$ and c = average composition vs. photon energy for Cu-Au alloys (from Ref. 28)

These authors claimed that when their data were corrected for lattice expansion, the 2.1 ev peak did not show any appreciable change in energy upon alloying.

Beaglehole and Whil[29,30] (1973) followed up their previous work with a discussion of screening charges and interactions between impurities in dilute metal alloys. In many of their measurements, changes in reflectance and the derived dielectric constant were found to vary in a non linear way, becoming linear only beyond several atomic precent of impurity. This was felt to be due to a transition from the situation of well separated, independent impurities at low concentrations to a situation of close interacting impurities at high concentrations. They plotted ε_{2ib} for Cu-Ga and Cu-Ge alloys and confirmed earlier findings by others that the threshold at 2.2 ev shifts to higher energies upon alloying. In Cu-Ga, the edge at 4.3 ev (which they associated with the threshold for conduction electron excitations) shifted to lower energies with alloying. They studied the region around 2.2 ev in detail by plotting $d(\omega^2\varepsilon_{2ib})/dE$ vs. E. This derivative is supposed to peak at an energy E, where transitions are taking place. In pure copper, a peak lies at 2.2 ev, corresponding to transitions from a flat portion of the d-band below the Fermi level to states above the Fermi level, and upon alloying, this peak drops in height without shifting in energy. At higher concentrantions, a second peak apparently develops at 2.32 ev and then shifts to higher energies. It has to be emphasized, however, that Beaglehole et al. employed a multistep evaluation process of their experimental data which could induce additional (i.e., non relevant) structure.

The behavior of absorption due to excitations from d-bands can be understood in terms of screening effects which were proposed by Friedel. The drop in the peak at 2.2 ev was interpreted to be due to a reduction in the number of copper atoms unperturbed by the impurities, i.e., those copper atoms at a distance from any impurities. At higher concentrations, all copper atoms may be affected by the impurities. Consequently, the screening charges must overlap. The authors speculated that at these concentrations, the secondary peak shifts to higher energies as the electronic structure of the host material begins to change.

Using positron annihilation experiments on Cu-Ge and Su-Si alloys, Suzuki et al.[31] (1974) studied the Fermi surface of these alloys. They concluded that upon alloying, the movement of the Fermi level relative to the top of the d-bands is small and, hence, the change in the

Fermi surface with alloying may be mainly induced by the change in the conduction band states near the Fermi level. They also discussed the model of conduction band sinking with increasing solute concentration relative to the Fermi level, which was proposed earlier by DeReggi and Rea.

Bansil, Ehrenreich et al.[32] (1974) calculated the energy bands for disordered α Cu-Zn for a 15 and 30at.% Zn alloy and examined the effects of charge transfer between atomic constituents. They applied their theoretical models to the appropriate experimental data of Pells and Montgomery, and concluded that the magnitude of the rise in the Fermi energy simply due to an increasing average number of electrons per atom from the solute is in reality less than one would predict, based on the rigid band model for copper. They considered two different models of charge transfer as possible causes for this discrepancy. They outlined the "shifted muffin tin" (SMT) and the "charge renormalized (CR) schemes." Each model involved an empirical parameter, whose value is adjusted to obtain agreement between the calculated and experimental values of the shift in the fundamental optical edge as a function of Zn concentration. They compared the shifts in the optical structure with concentration using both models.

The behavior of the 5 ev peak provided an independent test of their calculations.

In the SMT model, charge transfer has the effect of shifting all the levels of the alloy downwards compared to pure copper. In addition, a lowering of the conduction bands with respect to the d-bands resulted from the calculations. In the CR model, the d-bands rise because the copper atomic potential is raised. This also increases the Fermi energy slightly. An energy level diagram, which takes this into account, is presented in Figure 2.18. This diagram shows the effect on the bands of the alloy using these two models with respect to an alloy with no charge transfer (NA). This diagram also reveals that the principal effect of the adjustments involved in either the SMT or the CR models is to reduce the gap between the top of the d-bands and the Fermi level. Both models predict the $X_5 - X_{4'}$ and $L_1^{\ell} - E_F$ transitions to move to lower energies upon alloying faster than the $L_{2'} - L_1^{u}$ transition. The SMT model appeared to agree with the experimental shifts of Pells and Montgomery rather well, however, the authors feel that this better agreement compared to the CR model may be coincidental.

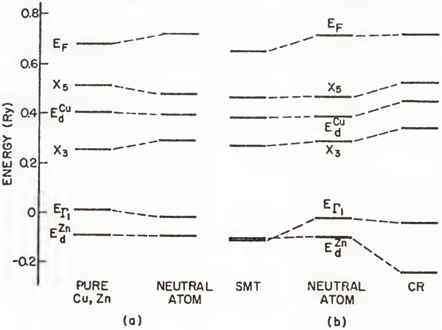

Figure 2.18. Energy level diagram for pure crystals and α-Cu 30at.% Zn
(a) pure crystals and Neutral Atom model
(b) Neutral Atom, SMT, and CR models (from Ref. 32)

II-5 Summary

The following tables summarize the main features observed in the optical spectrum of copper by various authors using different theoretical models and experimental techniques. Table 2.5 is a summary of peak assignment by authors and Table 2.6 is a summary of peak assignments by transition energies.

As can be seen from Table 2.6, there is general agreement that the transition observed in copper and its alloys around 2.0 - 2.5 ev is due to a d-band - Fermi energy transition. Whether it occurs near X or L is still a matter of controversy. However, it seems quite possible that this transition is indeed a combination of both transitions as well as a sum of all transitions from the flat upper d-bands to the Fermi surface over all regions of k space.

There is a large disagreement as to the assignment of higher energy structure, however. By observing Table 2.6, there appears to be a rather wide range (3.45 - 4.0 ev) of energies where observed structure is assigned to the X_5 - $X_{4'}$ transition. The lack of agreement on the exact energy here may be due to the different types of experimental techniques and theoretical models used for studying the electronic structure. It should be noted

Table 2.5

Assignment of Structure in the Optical Spectrum of Cu by Author

Author	Ref.	Technique	Energy	Transition Identification
Biondi and Rayne	3	Calorimetric	2.15 ev	$d \to E_F$
Ehrenreich and Philipp	5	Absorption	2.1 ev 5 ev	$L_3 \to L_{2'}(E_F)$ $X_5 \to X_{4'}$ $L_{2'} \to L_1$
Beaglehole	9	Absorption	2.5 ev 3.5 ev 5.5 ev	$d \to E_F$ lower $d \to E_F$
Gerhardt, Beaglehole and Sandrock	10	Piezo-optical	2 ev 3.9 ev 4.3 ev	$d \to E_F$ $X_5 \to X_{4'}$ $L_{2'} \to L_1$
Gerhardt	11	Reflection-strain	2.1 ev 4.0 ev 4.15 ev	$L_3 \to L_{2'}(E_F)$ $X_5 \to X_{4'}$ $E_F \to L_1{}^u$
Mueller and Phillips	12	Theoretical	2.1 ev 2.9 ev 4.8 ev 7.5 ev	$d \to E_F(x)$ $d \to E_F(L)$ $L_{2'} \to L_1$ $L_1{}^i \to L_{2'}(E_F)$
Dresselhaus	13	Theoretical	2.2 ev 4.2 ev	$d \to E_F$ lower $d \to E_F$

Table 2.5 - continued.

Author	Ref.	Technique	Energy	Transition Identification
Lettington	15	Absorption	2.2 ev	$L_3 \rightarrow L_{2'},(E_F)$
			3.45 ev	$L_{2'} \rightarrow L_1$
			4.3 ev	$X_5 \rightarrow X_{4'}$
Pells and Montgomery	17	Absorption	2.2 ev	$d \rightarrow E_F$
			4.8 ev	$L_{2'} \rightarrow L_1^{\,u}$
			5.4 ev	$L_1^{\,\ell} \rightarrow E_F$
Soven	18	Theoretical	3.88 ev	$X_5 \rightarrow X_{4'}$
			4.42 ev	$L_{2'} \rightarrow L_1$
Fong	19	Wavelength Modulation and Theoretical	2.1 ev	$\Delta_5 \rightarrow \Delta_1$
			3.2 ev	volume effect
			3.7 ev	$\Sigma_1 \rightarrow \Sigma_1(3\ 6)$
			3.7 ev	volume effect
			3.96 ev	$X_5 \rightarrow X_{4'}$
			4.25 ev	$L_{2'} \rightarrow L_1^{\,u}$
			4.38 ev	$\Sigma_1 \rightarrow \Sigma_1(1\text{-}6)$
			4.5 ev	volume effect
			5.0 ev	volume effect
Welkowsky and Braunstein	20	Wavelength Modulation	2.18 ev	$\Delta_5 \rightarrow \Delta_1$ & $L_3(Q_+) \rightarrow E_F(L_{2'})$
			2.53 ev	$L_2(Q_-) \rightarrow E_F(L_{2'})$
			3.75 ev	$X_5 \rightarrow X_{4'}$
			4.74 ev	$L_{2'} \rightarrow L_1$

Table 2.5 - continued.

Author	Ref.	Technique	Energy	Transition Identification
Williams, Janak and Moruzzi	21	Photoemission	4.2 ev	$L_{2'} \to L_1$
Das and Joshi	23	Theoretical	2.2 ev	$L_3 \to L_{2'} (E_F)$
			3.45 ev	$X_5 \to X_{4'}$
			4.3 ev	$L_{2'} \to L_1$
Rea and DeReggi	25 & 26	Absorption	2.2 ev	$d \to E_F$
			4.3 ev	$L_{2'} (E_F) \to L_1^{u}$
			5 ev	low $d \to E_F$
Rosei and Lynch	27	Thermomodulation	2.15 ev	$L_3 \to E_F$
			4 ev	$X_5 \to X_{4'}$
			4.8 ev	low $d \to E_F$
Beaglehole and Erlbach	28	Compositional Modulation	2.1 ev	$d \to E_F$
			3.9 ev	$X_5 \to X_{4'}$
			4.1 ev	$E_F \to L_1^{u}$
			4.3 ev	$L_{2'} \to L_1$
			4.8 ev	$L_1^{\ell} \to E_F$
Hummel, Holbrook and Andrews	33	Compositional Modulation	2.2 ev	$\Delta_5 \to \Delta_1$
			4.18 ev	$X_5 \to X_{4'}$
			4.5 ev	$L_{2'} \to L_1$

Table 2.6

Assignment of Structure in the Optical Spectrum of Cu by Energy

Gap Energy	Transition Assignment	Reference
2.0-2.5 ev	d-band Fermi energy around X or L	3,5,9-13,15,17,19,20,23,25-28,33
2.9 ev	d→E_F at L specifically	12
3.2 ev	volume effect	19
3.45-3.5 ev	lower d→E_F $L_{2'}\to L_1$ $X_5\to X_{4'}$	9 15 23
3.7-3.75 ev	$\Sigma_1\to\Sigma_1(3\text{-}6)$ volume effect $X_5\to X_{4'}$ $X_5\to X_{4'}$	19 19 20 23
3.88 ev	$X_5\to X_{4'}$	18
3.9-3.96 ev	$X_5\to X_{4'}$ $X_5\to X_{4'}$	10 19
4.0 ev	$X_5\to X_{4'}$ $X_5\to X_{4'}$	11 27
4.10 ev	$E_F\to L_1{}^u$	28
4.15 ev	$E_F\to L_1{}^u$	11

Table 2.6 - continued.

Gap Energy	Transition Assignment	Reference
4.18 ev	$X_5 \rightarrow X_{4'}$	33
4.2 ev	lower d→E_F	13
	$L_{2'} \rightarrow L_1$	21
4.25 ev	$L_{2'} \rightarrow L_1^u$	19
4.3 ev	$L_{2'} \rightarrow L_1$	10
	$X_5 \rightarrow X_{4'}$	15
	$L_{2'} \rightarrow L_1$	23
	$L_{2'} \rightarrow L_1$	28
4.38 ev	$\Sigma_1 \rightarrow \Sigma_1 (1-6)$	19
4.42 ev	$L_{2'} \rightarrow L_1$	18
4.5 ev	volume effect	19
	$L_{2'} \rightarrow L_1$	33
4.74 ev	$L_{2'} \rightarrow L_1$	20
4.8 ev	$L_{2'} \rightarrow L_1$	12
	lower d→E_F	27
	$L_1^{\ell} \rightarrow E_F$	28

Table 2.6 - continued.

Gap Energy	Transition Assignment	Reference
5.0 ev	$X_5 \rightarrow X_{4'}$	5
	$L_{2'} \rightarrow L_1$	
	volume effect	19
	lower $d \rightarrow E_F$	25,26
5 5.4 ev	$L_1{}^{\ell} \rightarrow L_{2'} (E_F)$	12
	$L_1{}^{\ell} \rightarrow E_F$	17

that although many authors assign this transition to structure observed in this energy region, there are those[12] who say that this transition is weak and will not show up in the optical spectrum of copper. Possibly this structure could be due to volume effects which was postulated[19] or also due to transitions from the Fermi energy to the upper L_1 band.

There is general agreement among authors that the $L_{2'} - L_1$ transition will be observed both in experimental measurements and in theoretical calculations. Structure assigned to this transition has been observed primarily between 4.2 and 4.8 ev. Again, there is disagreement as to the exact energy of the transition. It is felt by some[9,13,27,28] that transitions from the lower d-bands to the Fermi energy are also important in this energy region, that is $L_1^{\ell} - E_F$. If this is the case, then it seems probable that transitions from the middle of the d-bands to the Fermi energy should also be observed. These transitions may indeed be taking place, but due to the broadness of the structure at these energies, they may be masked. Structure which is observed at energies greater than 5 ev is specifically attributed to the lower d-band - Fermi energy transition. It is evident from the tables and the above discussion that there are many questions yet to be resolved in the interpretation and understanding of the optical properties of copper.

CHAPTER III
EXPERIMENTAL PROCEDURE

III-1 Sample Preparation

A major consideration in the preparation of the alloys used in this study was the maintenance of high purity. Therefore, the alloys were made from starting materials of the following purity:

Cu	99.999%
As	99.99%
Si	99.999%
Sn	99.999%
Au	99.99%
Al	99.999%

The copper was cleaned in a 50% nitric acid solution to assure removal of surface oxidation.

The alloy compositions made in this study are listed in Table 3.1. The alloy constituents were placed in vycor tubes and evacuated to approximately 10^{-2} Torr by a mechanical pump. The tubes were flushed repeatedly with Helium to ensure the removal of Oxygen. Finally, the tubes were backfilled with a sufficient quantity of Helium so that the pressure inside the tube during melting was approximately atmospheric. The amount of He left in the

Table 3.1

Alloy Compositions Prepared in This Study

System	at.% Solute
Cu-Au	0.5
	1
	2
	4
	7
	9
	12
	15
Cu-Al	0.1
	0.25
	0.5
	1
	1.5
	2
	3
	4
	5
	6
	7
	8
	9
	10
Cu-Si	0.5
	1
	1.5
	2
	3
	4
	6
Cu-Sn	0.5
	1
	1.5
	2
	3
	4
	5
Cu-As	0.5
	1
	2
	3
	4
	5

tube was determined using the ideal gas law. This was done to reduce the possibility of collapse of the tube and to prevent excessive bubble formation during melting. Special precaution had to be taken in the case of the Copper-Arsenic samples since Arsenic sublimes at 603°C. Therefore, these samples were sealed under vacuum.

The alloys were melted using an induction furnace, and heated very rapidly (i.e., molten in approximately 20 sec) to prevent sticking of the material to the side of the tube. The alloys were held in the molten state for approximately 3 - 4 minutes. Prior to turning off the power of the furnace, the tubes were shaken to eliminate any bubbles which might have formed. The samples were air cooled in the vycor tubes. After removal, most of the alloys looked shiny. On rare occasions, some alloys showed slight surface oxidation due to the cracking of the vycor tubes in the latter stages of cooling. These samples were cleaned by sandblasting the surface and rinsing in acetone.

The alloys were then cold rolled to a thickness of 3 mm to induce cold work (to increase diffusion) and also to reduce the diameter. They were then resealed in vycor tubes, this time under vacuum of 10^{-2} Torr, and placed into a furnace for approximately 10 - 14 days for homogenization slightly below the solidus temperature. The time allowed is sufficient to eliminate any coring and to produce a homogeneous alloy as could be substantiated by differential reflectograms on a single alloy.

After the above treatment, the samples were cold rolled again, to 1 mm thickness, and then given an annealing treatment for one hour at 600°C. This served to produce a uniform grain size. The Cu-Sn alloys were not allowed to furnace cool, but were rather quenched to prevent precipitation of a second phase. The alloys were then cut on a diamond wheel to the proper size with utmost care to prevent any substantial deformation.

Two alloys with the same type solute but of slightly different composition were then cold mounted side by side with as small a gap as possible in between.

The samples were then polished using standard metallographic procedures. Rough grinding was done on 180 - 600 grit silicon carbide grinding paper, followed by final polishing with 6 μ and 1 μ diamond polishing compound on felt cloth.

The polished samples were rinsed with high purity methanol and swabbed with cotton to insure that no oil film from the polishing liquid remained on the surface.

The samples were immediately taken to the differential reflectometer and a differential reflectogram was thus obtained within 3 - 5 minutes after polishing.

III-2 Experimental Setup - The Differential Reflectometer

A detailed description of the differential reflectometer was given by Holbrook and Hummel.[34] In the present study, an improved version was used employing mirrors instead of lenses and a monochromator with a higher resolution (see Figure 3.1).

The primary function of the differential reflectometer is to measure the difference in reflectivities between two samples of slightly different composition. The present apparatus is capable of measuring over the spectral range from 800 to 200 nm.

Light from a high pressure Xe source passes through a monochromator and falls on a mirror which is vibrating at a frequency of 60 Hz (Figure 3.1). This mirror causes the light beam to be alternately scanned from one sample to the other. The vibrating mirror is concave and focuses the light from the exit slit of the monochromator onto the sample plane. The light which is reflected from the sample impinges on a second concave mirror which focuses the vibrating mirror onto a quartz disc which is placed

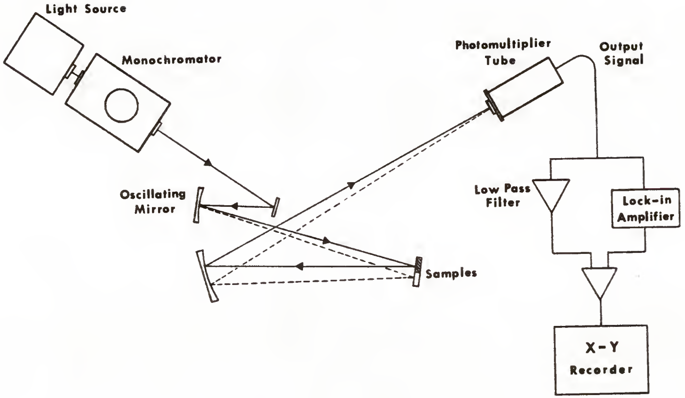

Figure 3.I. Schematic Diagram of the optical and electronic components of the differential reflectometer

in front of the photomultiplier tube (PMT). The function of the quartz disc is to disperse the light evenly over the surface of the PMT. The signal from the PMT is electronically processed to obtain the normalized difference in reflectivities between the two samples.[34] This is done by using a lock-in amplifier which provides an output proportional to the difference in reflectivities between the two samples, ΔR. To eliminate fluctuations in light intensity and other equipment variations, ΔR is normalized by dividing by the average reflectivity, $\bar{R} = (R_1 + R_2)/2$. This is done by a signal averaging and dividing circuit. $\Delta R/\bar{R}$ as a function of wavelength is plotted by means of an X-Y recorder. The resultant plot will from now on be referred to as a differential reflectogram.

CHAPTER IV
THEORETICAL BACKGROUND

IV-1 Relationship of Optical Properties to Electronic Structure

As outlined in the Introduction, the optical properties are directly related to the electronic structure of a solid. The details of this interrelationship will be discussed in this section.

The optical properties of metals are defined by the complex index of refraction $\hat{n}$,

$$\hat{n} = n - ik$$

where n is the index of refraction and k is the absorption coefficient of the metal. These material constants can be measured by conventional optical techniques (ellipsometry).[35]

The complex index of refraction $\hat{n}$ is related to the complex dielectric function $\hat{\varepsilon}$ by the Maxwell relation

$$\hat{n}^2 = \hat{\varepsilon}$$

where $\hat{\varepsilon}$ can be expressed in terms of its real and imaginary parts by

$$\hat{\varepsilon} = \varepsilon_1 - i\varepsilon_2$$

where ε_1 (polarization), and ε_2 (absorption) are connected to n and k by

$$\varepsilon_1 = n^2 - k^2$$

$$\varepsilon_2 = 2nk$$

The above two equations then relate the optical constants to the electronic properties of the metal.

The quantity usually measured in most optical experiments involving metals is the reflectivity R. The reflectivity can be expressed in terms of the optical constants by the Beer's equation,

$$R = \frac{(n-1)^2 + k^2}{(n+1)^2 + k^2}$$

and also in terms of the dielectric constants through the Fresnel equation,

$$R = \frac{(\varepsilon_1^2+\varepsilon_2^2)^{1/2} - [2\varepsilon_1 + 2(\varepsilon_1^2+\varepsilon_2^2)^{1/2}]^{1/2} + 1}{(\varepsilon_1^2+\varepsilon_2^2)^{1/2} + [2\varepsilon_1 + 2(\varepsilon_1^2+\varepsilon_2^2)^{1/2}]^{1/2} + 1}$$

By measuring the reflectivity of a metal over a large energy range, ε_1 and ε_2 can be determined by a Kramers-Kronig analysis.[36] The Kramers-Kronig relations connecting ε_1 and ε_2 are

$$\varepsilon_1(\omega_o) = 1 + \frac{2}{\pi} \int_o^\infty \frac{\omega \cdot \varepsilon_2(\omega)}{\omega^2 - \omega_o^2} d\omega$$

$$\varepsilon_2(\omega_o) = -\frac{2}{\pi} \omega_o \int_o^\infty \frac{\varepsilon_1(\omega) - 1}{\omega^2 - \omega_o^2} d\omega$$

There also exists a relationship between the real and the imaginary parts of the complex reflection amplitude $r = |r|e^{-i\phi}$ with $R = |r^2|$:

$$\phi(\omega_o) = \frac{1}{2\pi} \int_o^\infty \ell n \left|\frac{\omega-\omega_o}{\omega+\omega_o}\right| \frac{d}{d\omega} \ell n |R(\omega)| \, d\omega$$

ϕ can also be expressed as a function of ε_1 and ε_2. If R has been measured over a sufficiently large energy range, ϕ can be determined from the above equation. With both R and ϕ known, ε_1 and ε_2 can then be determined.

On an atomic scale, the absorption of light (or absorption of photons) involves the transition of electrons from a lower, filled energy state to a higher, unfilled state. Thus, the quantity most directly connected to these transitions is the imaginary part of the dielectric constant ε_2 (i.e., the absorption). The spectral dependence of ε_2 shows features of the energy band structure that optical measurements can investigate.

When monochromatic light is incident upon a material, certain electronic transitions will take place which can be located in the band structure of that material. (See Figure 2.2 which presents the band structure of copper.) The initial states or filled bands are seen to be below E_F. As mentioned above, photon absorption lifts an electron from an initial state with energy E_i and wave vector k to an empty band above E_F of energy E_f and wave vector k'. Transitions will only occur when the photon energy matches certain energy differences between the initial and final states. Because of conservation of momentum, the assumption of direct transitions, that is k = k', is usually made for metals.

Due to the nature of the joint density of states function,

$$J(\Delta E) = \frac{2}{(2\pi)^3} \int_{\Delta E=\mathrm{const}} \frac{ds}{|\nabla_k(\Delta E)|},$$

certain transitions are more probable than others. Points where $\nabla_k(\Delta E) = 0$ are particularly important. In such a case, the denominator of the integrand in the above equation is zero, and the joint density of states function, i.e., $J(\Delta E)$ vs. ΔE, shows a discontinuity in its slope. This point of discontinuity is called a "critical point."

There are two different types of critical points, in other words, there are two different ways in which the condition $\nabla_k(\Delta E) = 0$ can be met. The first way is for the lines E_i and E_f to be parallel, but not horizontal. Such an interval of near parallelism offers a large number of transition possibilities to photons in the energy range $E_f - E_i$. This can occur anywhere in the Brillouin Zone (BZ). Such a critical point is called a "general" critical point.

The second condition for $\nabla_k(\Delta E)$ being equal to zero is if both $\nabla_k(E_f)$ and $\nabla_k(E_i)$ vanish separately, as when the gradients are horizontal. This is a necessary condition at the edges of the BZ for reasons of symmetry.[37] Such a critical point is called a "symmetry" critical point.

Critical points not only introduce slope discontinuities into the joint density of states function, as mentioned above, but also produce slope changes in ε_2. These slope discontinuities can be correlated to the band separation at points of high symmetry in the BZ. Since these critical points have an effect on ε_2, they serve as a link between the band structure of the material and the optical experiments.

IV-2 Relationship of Differential Reflectograms With Interband Absorption

This section discusses the change in reflectance of a metal which is caused by small additions of alloying elements. In the present work, the solute concentration was changed periodically (by scanning a light beam between two samples of different alloy composition). Therefore, the technique is called compositional modulation.

Conventional spectral reflectance measurements of a metal, as shown in the Introduction, lack sharp structure, due to the spreading of energy levels to energy bands in a solid. However, by using a modulation technique, sharp structure can be obtained due to changes in the band structure at points of electron transitions caused by the change in alloy composition. Thus, modulation techniques separate out the singularities from the background.

As was shown previously, the reflectance can be described by the real and imaginary parts of the dielectric constant, ε_1 and ε_2, respectively. Hence, in a modulation technique, it is expected to observe a change in both ε_1 and ε_2.

In order to get some insight into the nature of modulation techniques (which essentially provide a derivative of the reflectivity with respect to the modulated parameter, in our case composition), it is helpful to differentiate the Fresnel equation (see previous section) with respect to the modulated parameter. This yields to

$$\frac{\Delta R}{R} = \alpha \frac{d\varepsilon_1}{dx} + \beta \frac{d\varepsilon_2}{dx} \tag{1}$$

where α and β are complex functions of ε_1 and ε_2 and are referred to as the Seraphin Coefficients.[37] They are expressed as

$$\alpha = C_1\ [(\varepsilon_1-1)\ A_+ + \varepsilon_2\ A_-],\ \beta = C_2\ [(\varepsilon_2-1)/A_+ - \varepsilon_2/A_-]$$

where

$$A_\pm = \pm\sqrt{2}[(\varepsilon_1^2+\varepsilon_2^2)^{1/2} \pm \varepsilon_1]^{1/2}$$

and

$$C_1 = [(\varepsilon_1-1)^2 + \varepsilon_2^2]^{-1}$$

$$C_2 = 2\varepsilon_2/[(\varepsilon_1-1)^2 + \varepsilon_2^2]\ (\varepsilon_1^2+\varepsilon_2^2)$$

The variable x in the differentiated equation above refers to the modulated parameter, in this work, the change in the composition of the alloy.

A legitimate question which arises immediately is the question about the correlation between a certain peak (or structure) in a differential reflectogram and a certain interband transition. The only way to accurately answer this is to write an equation for the reflectivity for a specific interband transition and to calculate the derivative of this reflectivity with respect to the modulated parameter, here, to the composition. By such a "line shape analysis," a possible confirmation between theory and experiment can be obtained. Also, based on certain other parameters in the theory, the exact energy for the electron transitions in the material can be obtained from the structure in the differential reflectogram. Such a calculation was done recently by Enderlein[38] for the low energy peak in the experimental reflectograms. Details of this calculation will be presented below.

The first step is to express the relationship between $\Delta R/R$ and the complex dielectric function $\hat{\varepsilon}$. We write

$$\Delta R = \frac{dR}{dx}\,\Delta x \tag{2}$$

where

x = composition

R = reflectivity

Since, as mentioned above, R is a function of ε_1 and ε_2 (i.e., the real and imaginary parts of the dielectric constant, respectively), we can note

$$R = R(\varepsilon_1(x),\ \varepsilon_2(x)) \tag{3}$$

This yields to

$$\frac{dR}{dx}/R = \left(\frac{dR}{d\varepsilon_1}\,\frac{d\varepsilon_1}{dx} + \frac{dR}{d\varepsilon_2}\,\frac{d\varepsilon_2}{dx}\right)/R \tag{4}$$

$\Delta R/R$ is related to $\frac{d\varepsilon_1}{dx}$ and $\frac{d\varepsilon_2}{dx}$ by the Seraphic Coefficients [Equation (1)]

$$\frac{\Delta R}{R} = \alpha\,\frac{d\varepsilon_1}{dx} + \beta\,\frac{d\varepsilon_2}{dx} \tag{1}$$

Certain assumptions have to be made on the mechanisms which determine the dielectric function in the energy region of a certain peak in the differential reflectogram;

in the case treated here, peak "A" has been chosen.

1. Peak "A" is caused by transitions between the d-bands and s states just above the Fermi level. (See Figure 4.1.)
2. Bands E_s and E_d are assumed to be isotropic. That is, the surfaces of constant energy are spherical.
3. The Fermi level changes with composition (x)
$$E_F = E_F(x)$$
4. The energy bands do not change with composition. That is, the rigid band model is assumed for simplification. (It is assumed that a change of E_s and E_d with x has a much weaker influence on the dielectric function $\hat{\varepsilon}$ than the change of E_F).
5. It is assumed that the momentum matrix elements or the oscillator strength of the transition under consideration does not change considerably with x.
6. The dielectric function can be described using the one-electron approximation. The scattering of Bloch-electrons can be taken into account by means of a lifetime broadening, Γ, of the energy

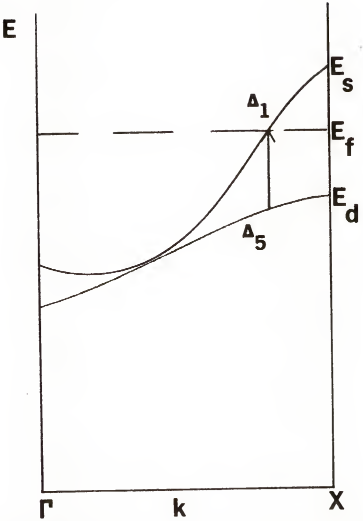

Figure 4.1. Transition $\Delta_5 \rightarrow \Delta_1$ corresponding to peak "A" in the differential reflectograms

bands:

$$\Gamma = \Gamma(k)$$

7. Only the interband part of the dielectric function is important in the frequency range under consideration.

8. The density of states function is assumed to be constant in the vicinity of the Fermi energy and is therefore not included in Equation (5).

The quantum mechanical equation for the dielectric function is noted below.

$$\varepsilon = \frac{4\pi e^2 i}{\hbar\omega^2 m^2} \int_{BZ} d^3k \frac{[f(E_d(k)) - f(E_s(k)]}{\hbar\omega - \{E_s(k) - E_d(k)\} + i\hbar\Gamma(k)} \qquad (5)$$

where f is the Fermi distribution function.

$$f(E) = \frac{1}{\exp(\frac{E-E_F}{kt}) + 1} \qquad (6)$$

In order to obtain $\frac{\Delta R}{R}$, we need, according to Equation (4), a value for $\frac{d\varepsilon}{dx}$. The only quantity in Equation (5) which depends on x is E_F and the only quantity which depends on E_F is $f(E_s(k))$, where

$$f(E_s(k)) = \frac{1}{\exp\ (\frac{E_s(k)-E_F}{kt}) + 1} \qquad (7)$$

This function has the form shown in Figure 4.2a, and $df(E_s)/dE_s$ has the form shown in Figure 4.2b. In order to

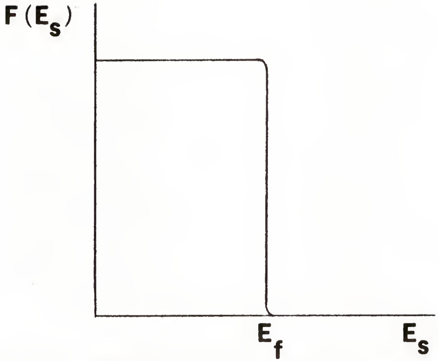

Figure 4.2a. Fermi Distribution Function

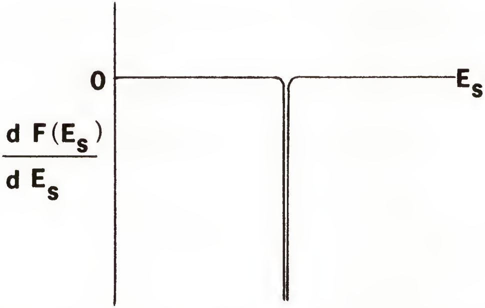

Figure 4.2b. Derivative of Fermi Distribution Function with respect to E_s

obtain $\frac{d\varepsilon}{dx}$, we need

$$\frac{df}{dx} = \frac{df}{dE_F} \cdot \frac{dE_F}{dx} \tag{8}$$

From Figure 4.2, it can be seen that $\frac{df}{dE_s}$ can be approximated using the Dirac delta function,

$$\frac{df}{dE_s} = -\delta(E_s(k) - E_F) \tag{9}$$

and from the symmetry of Equation (7), it can be seen that

$$\frac{df}{dE_s} = -\frac{df}{dE_F}$$

Thus,

$$\frac{df}{dE_F} = +\delta(E_s(k) - E_F) \tag{10}$$

Substituting Equation (10) into Equation (8),

$$\frac{df}{dx} = +\delta(E_s(k) - E_F) \cdot \frac{dE_F}{dx} \tag{11}$$

With this, and defining $E_s(k) - E_d(k) = E_{sd}$, one can write

$$\frac{d\varepsilon}{dx} = \frac{4\pi e^2 i}{\hbar\omega^2 m^2} \cdot \frac{dE_F}{dx} \int d^3k \{\frac{\delta(E_s(k) - E_F)}{\hbar\omega - E_{sd}(k) + i\hbar\Gamma(k)}\} \tag{12}$$

As a consequence of the assumption that the bands are isotropic, a transformation to spherical coordinates can be made, which yields

$$d^3k = 4\pi k^2 \; dk \tag{13}$$

and Equation (12) reads

$$\frac{d\varepsilon}{dx} = \frac{(4\pi)^2 e^2 i}{\hbar\omega^2 m^2} \quad \frac{dE_f}{dx} \int_0^\infty dk\ k^2\ f(k)\ \delta(E_s(k) - E_F) \quad (14)$$

where

$$f(k) = \frac{1}{\hbar\omega - E_{sd}(k) + i\hbar\Gamma(k)} \quad (15)$$

To perform the integration of Equation (15), one has to change variables because the delta function is defined in terms of the variable E_s. Since E_s is a function of k,

$$E_s = E_s(k)$$

one obtains

$$dE_s = \frac{dE_s}{dk} \cdot d\ k$$

Therefore,

$$dk = dE_s \cdot \frac{1}{(\frac{dE_s}{dk})} \quad (16)$$

Substituting Equation (16) into Equation (14),

$$\frac{d\varepsilon}{dx} = \frac{(4\pi)^2 e^2 i}{\hbar\omega^2 m^2} \cdot \frac{dE_f}{dx} \int_0^\infty f(k) k^2 \frac{1}{(\frac{dE_s}{dk})} \delta(E_s(k) - E_F) \cdot dE_s \quad (17)$$

Since $f(k)\ k^2 \cdot \frac{1}{(\frac{dE_s}{dk})}$ is a function of E_s, let it be equal to $g(E_s)$. Equation (17) now reads

$$\frac{d\varepsilon}{dx} = \frac{(4\pi)^2 e^2 i}{\hbar\omega^2 m^2} \cdot \frac{dE_F}{dx} \int_0^\infty g(E_s)\ \delta(E_s(k) - E_F) dE_s \quad (18)$$

Knowing for delta functions that

$$\int_0^\infty g(u)\ \delta[u - c]du = g(c), \tag{19}$$

integrating the integrand in Equation (18), we get

$$\int_0^\infty g(E_s)\ \delta(E_s(k) - E_F) \cdot dE_S = g(E_F) \tag{20}$$

Substituting Equation (20) into Equation (18),

$$\frac{d\varepsilon}{dx} = \frac{(4\pi)^2 e^2 i}{\hbar m^2 \omega^2} \cdot \frac{dE_F}{dx} \left[f(k_F) \cdot k_F^2 \cdot \frac{1}{\left(\frac{dE_s}{dk}\right)_{k=k_F}}\right] \tag{21}$$

Since $E_s(k_F) - E_F = 0$, we obtain $E_F = E_S$ and $k = k_F$. This yields

$$\frac{d\varepsilon}{dx} = \frac{(4\pi)^2 e^2 i}{\hbar m^2 \omega^2} \frac{dE_F}{dx} \left[\frac{k_F^2}{\left(\frac{dE_s}{dk}\right)_{k=k_F}} \cdot \frac{1}{\hbar\omega - E_{sd}(k) + i\hbar\Gamma(k)}\right] \tag{22}$$

Define $\hbar\omega_T$ to be equal to the transition energy, E_{sd}, which may or may not depend on composition.

$$E_{sd} = \hbar\omega_T \tag{23}$$

Substituting Equation (23) into Equation (22) and multiplying by $\hbar$ yields

$$\frac{d\varepsilon}{dx} = \frac{(4\pi)^2 e^2}{\hbar^2 \omega^2 m^2} \quad \frac{dE_F}{dx} \cdot \frac{k_F^2}{\left(\frac{dE_s}{dk}\right)_{k=k_F}} \cdot \frac{i}{(\omega - \omega_T) + i\Gamma(k)} \tag{24}$$

Define

$$\frac{(4\pi)^2 e^2}{\hbar^2 \omega^2 m^2} \cdot \frac{k_F^2}{(\frac{dE_s}{dk})_{k=k_F}} = k > 0 \tag{25}$$

Therefore,

$$\frac{d\varepsilon}{dx} = +k \frac{dE_F}{dx} \cdot \frac{i}{(\omega-\omega_T)+i\Gamma(k)} \tag{26}$$

This equation is the basis for the interpretation of the $\Delta R/R$ line shape. Now, it is necessary to fit the theoretical and experimental $\Delta R/R$ spectra.

It can be shown (Appendix 1) that

$$\Delta R/R = \alpha\frac{d\varepsilon_1}{dx} + \beta\frac{d\varepsilon_2}{dx} \tag{1}$$

is identical with

$$\Delta R/R = \mathrm{Re}\{ce^{i\Theta}\frac{d\varepsilon}{dx}\} \tag{27}$$

Inserting Equation (26) into Equation (27) yields

$$\frac{\Delta R}{R} = +k \frac{dE_F}{dx} c \ \mathrm{Re}\{e^{i\Theta} \frac{i}{(\omega-\omega_T)+i\Gamma(k)}\} \tag{28}$$

Define $$s = \frac{\omega-\omega_T}{\Gamma(k)} \tag{29}$$

Therefore $$\omega-\omega_T = \Gamma(k)s \tag{30}$$

Substituting Equation (30) into Equation (28),

$$\frac{\Delta R}{R} = +k \frac{dE_F}{dx} c \ \mathrm{Re}\{e^{i\Theta} \frac{i}{\Gamma(k)s+i\Gamma(k)}\} \tag{31}$$

Rearranging terms,

$$\frac{\Delta R}{R} = +\frac{kc}{\Gamma}\frac{dE_F}{dx}\,\mathrm{Re}\{e^{i\Theta}\,\frac{i}{s+i}\} \tag{32}$$

It can be shown (Appendix 2) that

$$\frac{i}{s+i} = \frac{1}{\sqrt{s^2+1}}\,e^{i(\pi/2-\phi)} \tag{33}$$

Substituting Equation (33) into Equation (32) yields

$$\frac{\Delta R}{R} = +\frac{kc}{\Gamma}\frac{dE_F}{dx}\,\mathrm{Re}\{e^{i\Theta}\cdot\frac{e^{i(\pi/2-\phi)}}{\sqrt{s^2+1}}\} \tag{34}$$

Rearranging Equation (34) yields

$$\frac{\Delta R}{R} = +\frac{kc}{\Gamma}\frac{dE_F}{dx}\,\mathrm{Re}\{e^{i(\Theta-\phi+\pi/2)}\}\frac{1}{\sqrt{s^2+1}} \tag{35}$$

Since

$$\mathrm{Re}\{e^{i(\Theta-\phi+\pi/2)}\} = \cos(\Theta-\phi+\pi/2) = -\sin(\Theta-\phi) \tag{36}$$

and $\frac{1}{\sqrt{s^2+1}} = \sin\phi$ (see Appendix 2), we obtain

$$\frac{\Delta R}{R} = -\frac{kc}{\Gamma}\frac{dE_F}{dx}\,\sin(\Theta-\phi)\,\sin\phi \tag{37}$$

Let

$$A = -\frac{kc}{\Gamma} \tag{38}$$

and

$$F(s) = \sin(\Theta-\phi)\,\sin\phi \tag{39}$$

Substituting Equation (38) and Equation (39) into Equation (37) yields

$$\frac{\Delta R}{R} = +A \frac{dE_F}{dx} F(s) \tag{40}$$

This equation expresses the relationship between $\frac{\Delta R}{R}$ and F(s) for peak "A" in the reflectograms. When the function F(s) is plotted vs. s, different curve shapes are obtained which can be compared with the experimental $\frac{\Delta R}{R}$ curves. The function F(s) can be found by calculating $F(s) = \sin(\Theta-\phi)\sin\phi$ for different values of Θ where $\Theta = \arctan\beta/\alpha$. Plots of F(s) for Θ values ranging from 0° to 360° are shown in Figure 4.3 As can be seen by comparing our experimental differential reflectograms with Figure 4.3, the interesting Θ range for peak "A" is $90° < \Theta < 180°$. For $\Theta = 180°$, $F(s) = \sin^2\phi$ and the F(s) curve is symmetrical around $s = 0$. In this case, the peak frequency, ω_M, is equal to the transition frequency ω_T. For $\Theta = 90°$, $F(s) = \sin\phi\cos\phi$ and F(s) is asymmetrical about $s = 0$ and ω_T lies to the left of ω_M at $s = 0$, i.e., in the middle between the minimum and the maximum. For all other values of Θ, the true transition frequency, ω_T, has to be found by a line shape analysis. This is done in the next section.

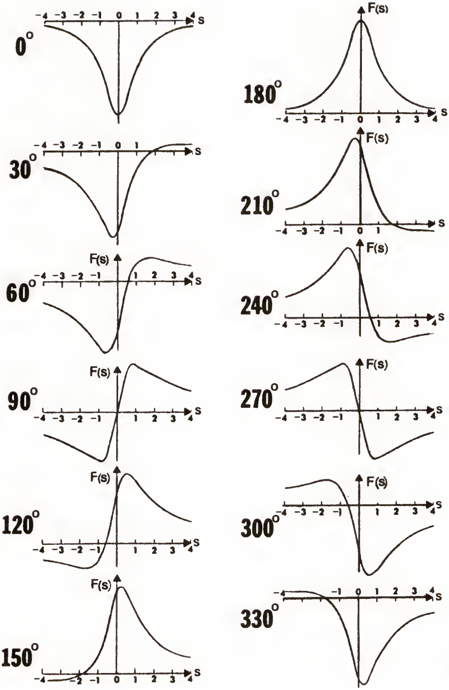

Figure 4.3. F(s) vs. s for Θ values from 0° to 330°

IV-3 Line Shape Analysis

This section deals with the line shape analysis of the first peak in the differential reflectograms (peak "A" and vicinity), that is, the peak which is generally assigned to transitions from the top of the d-bands to the Fermi energy. Calculated curves for $\frac{\Delta R}{R}$, or better F(s) versus s (i.e., essentially energy), and the procedure of matching their line shapes with those of the experimental curves in order to determine the exact transition energy (E_T) will be presented.

Figure 4.4 shows the calculated curves of F(s) plotted as a function of S where $S = (\omega-\omega_T)/\Gamma$. The parameter $\tan\Theta$ is the ratio of the Seraphin coefficients β and α (i.e., $\tan\Theta = \beta/\alpha$), and was varied from 90°- 180° in increments of 5°. As can be seen, the F(s) curve for Θ = 90° shows an asymmetrical behavior, while for Θ = 180°, one obtains a symmetrical curve around the transition frequency ω_T. This means that for Θ = 180°, ω_T is identical with the frequency of the maximum of the peak (peak "A"). As Θ deviates from 180°, the transition frequency, ω_T, becomes smaller compared to the location of peak "A." A correction has therefore to be undertaken in all cases where $\Theta \neq 180°$.

The first step which much be performed in the cor-

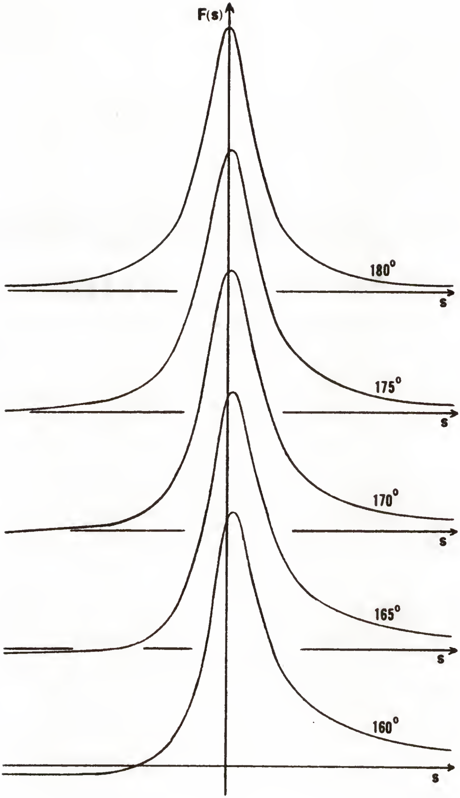

Figure 4.4. Calculated F(s) curves as a function of s for Θ between 90 and 180° in increments of 5°

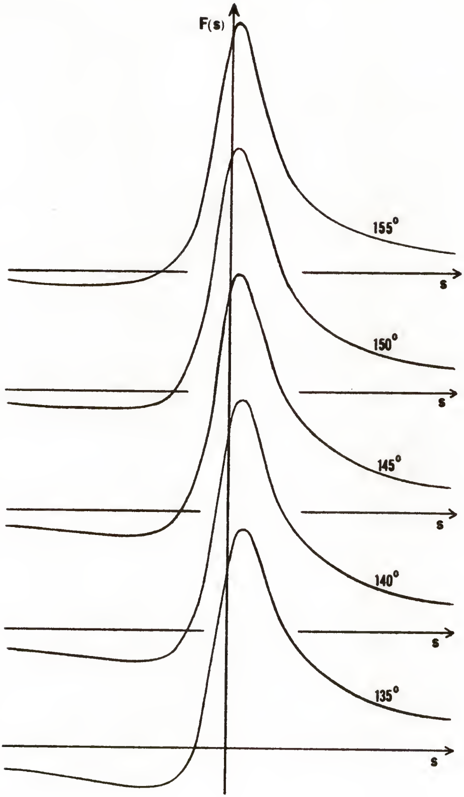

Figure 4.4 - continued

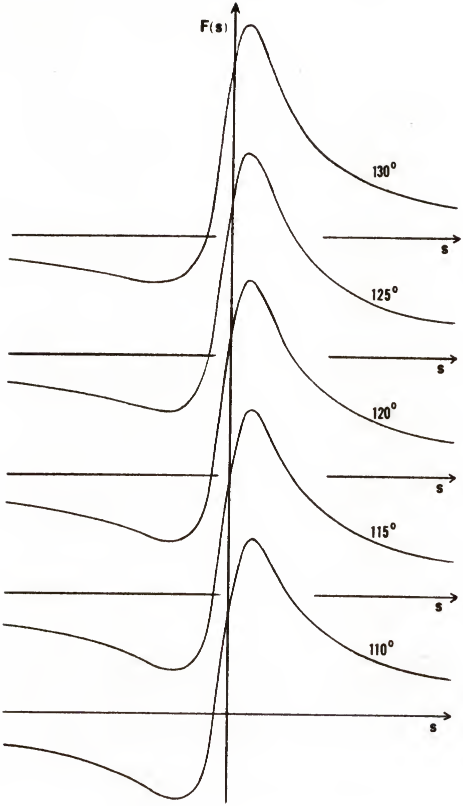

Figure 4.4 - continued

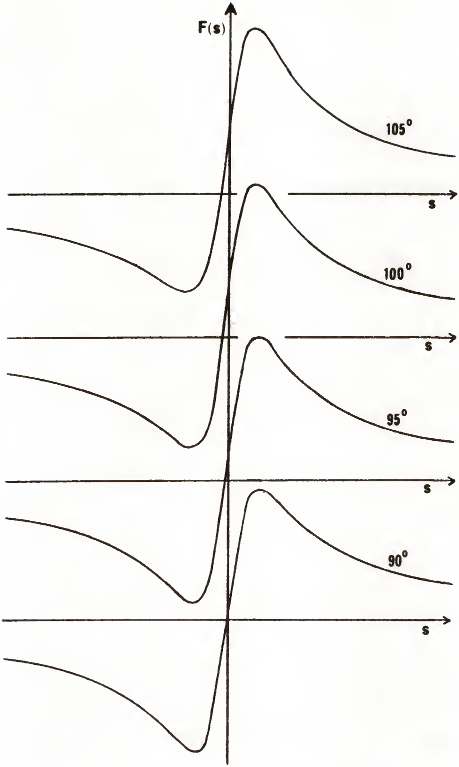

Figure 4.4 - continued

rection procedure is to characterize the line shapes of the calculated curves so that the experimental curves can later be compared to them. The characterization of these calculated curves is outlined below. Reference to Figure 4.5 is made.

1. A horizontal line (1) is drawn tangent to the minimum in the F(s) vs. S curve. This is used as a zero line reference.
2. The S value at the peak maximum is denoted as S_M and the corresponding point on the F(s) axis is termed $F(S_M)$.
3. A horizontal line is drawn at $1/2\ F(S_M)$.
4. The corresponding S value (denoted S') is marked.
5. The distance $(S_M - S')$ is defined as ΔS.
6. Mark the value $S_M + \Delta S$, which is called S''.
7. Measure F(S) at S'', which is termed F(S'').
8. Take the ratio $F(S'')/F(S_M)$.

This procedure was performed for various Θ values in 5° increments between $\Theta = 90°$ and $\Theta = 180°$. The ratio $F(S'')/F(S_M)$ is plotted as a function of Θ in Figure 4.6. In the computer plots (Figure 4.4), the vertical axes represent the actual transition energy or, in this particular case, the quantity S_T. In order to relate S_T to a certain curve type

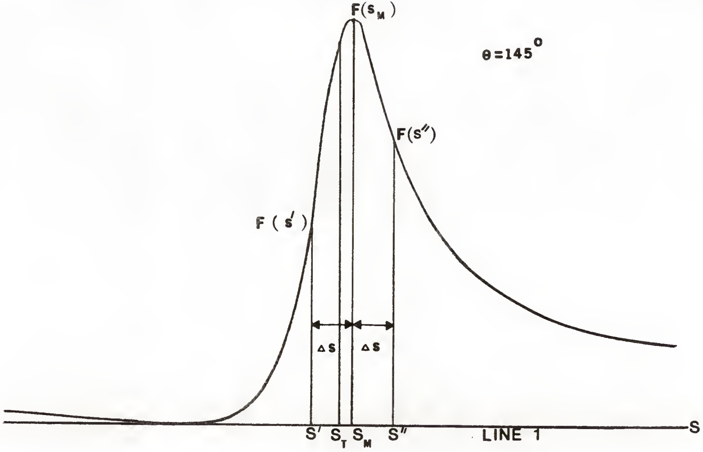

Figure 4.5. Plot of F(s) vs. s for a Θ value of 145°

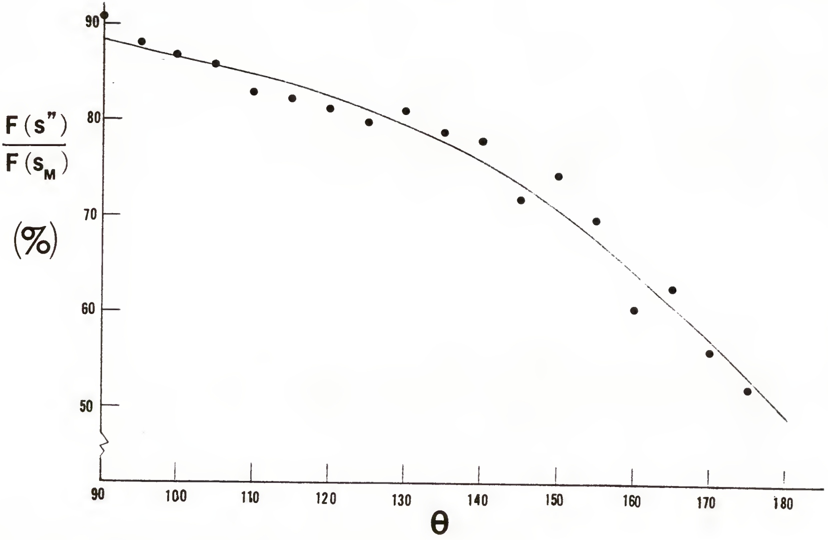

Figure 4.6. Plot of $F(S'')/F(S_M)$ vs. Θ

(or, specifically, to Θ), one has to perform the following procedure.

Take the ratio of $(S_M - S_T)/\Delta S$, which will be defined to be R. Plot R as a function of Θ (see Figure 4.7). This ratio will provide the correction factor needed to determine the actual transition energy from the experimental curves. For this, one has to perform similar operations on the experimental curves, that is one has to first determine the ratio $F(E'')/F(E_M)$ in order to determine Θ. Then, from the Θ value and Figure 4.7, the corrected transition energy can be obtained.

A sample analysis on a differential reflectogram for a Cu-1% Al alloy follows, with reference being made to Figure 4.8.

1. The base line is drawn, touching the minimum point.
2. The peak maximum, E_M, is equal to 2.207 ev.
3. By drawing a horizontal line at $F(E') = 1/2\ F(E_M)$, $\Delta E = (E_M - E')$ is determined to be .0718 ev.
4. The ratio of $F(E'')/F(E_M)$ is found to be 72%.
5. Referring to Figure 4.6, the value of Θ is 148°.
6. Using Figure 4.7, the correction factor for Θ = 148° can be found to be R = 0.31.

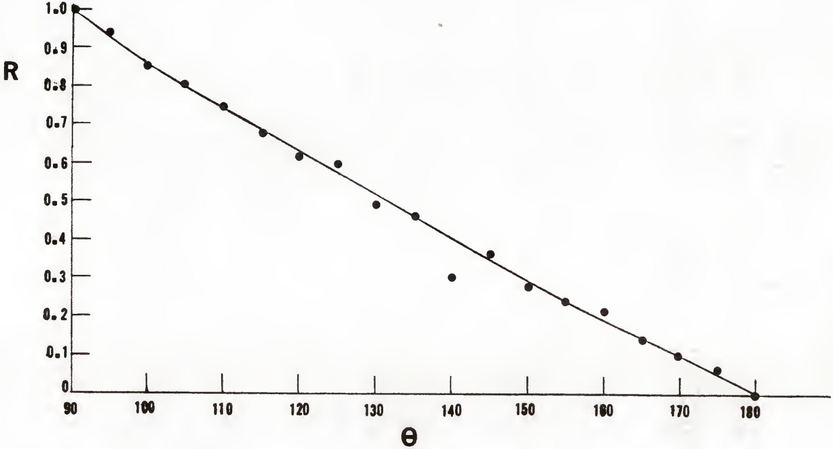

Figure 4.7. Correction factor R as a function of Θ

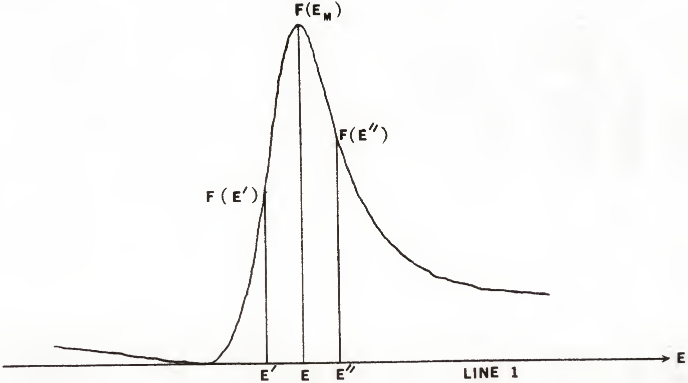

Figure 4.8. Differential Reflectogram of Cu-lat.% Al in the region of peak "A"

7. With $R = \frac{S_M - S_T}{S_M - S'} \equiv \frac{\Delta S_T}{\Delta S} \equiv \frac{\Delta E_T}{\Delta E}$ (see Figure 4.5), and taking ΔE from the experimental curve, one obtains $E_T = 0.0223$ ev, which has to be subtracted from the maximum energy, E_M, to obtain the corrected transition energy, $E_T = 2.185$ ev.

CHAPTER V
EXPERIMENTAL RESULTS

The objective of this work was to systematically investigate the optical properties of all suitable α-phase copper based alloys, and to relate the results to existing theories on alloy behavior and electronic structure. The alloys used in this study are marked in bold lines in a section of the Periodic Table (Figure 5.1). The other elements in the vicinity of copper had too low a solubility in copper so that useful alloys could not be made. Since the studies which are reported here are a continuation of the work done by Holbrook[39] and Andrews,[40] some of the alloys have been already available. They have been remeasured, nevertheless, because an improved version of the differential reflectometer has been used for this work. This eliminated the possibility of systematic errors which could have been introduced due to the change in equipment.

The experimental results in the form of the differential reflectograms of the alloys are presented in the following figures (Figure 5.2 - 5.8). By inspecting a typical differential reflectogram, for example the one presented in Figure 5.3, four distinct peaks can be ob-

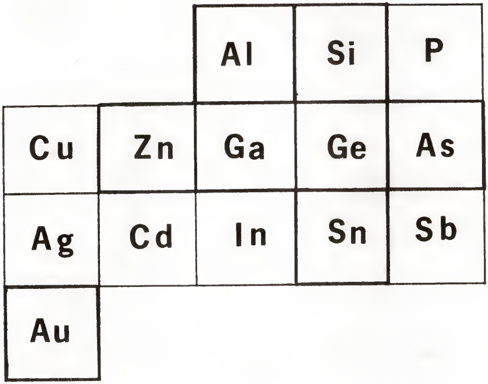

Figure 5.1. Elements used in this study for alloying with copper (bold lines)

Figure 5.2. Differential Reflectograms for various Cu-Zn alloys

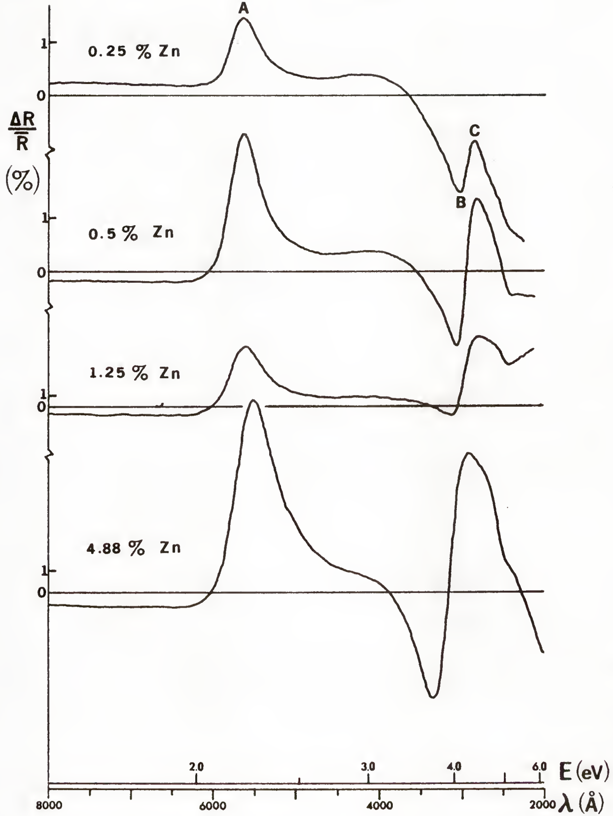
A
B
C
0.25 % Zn
0.5 % Zn
1.25 % Zn
4.88 % Zn
ΔR/R (%)
1
0
2.0
3.0
4.0
6.0
E (eV)
8000
6000
4000
2000
λ (Å)

Figure 5.2 - continued

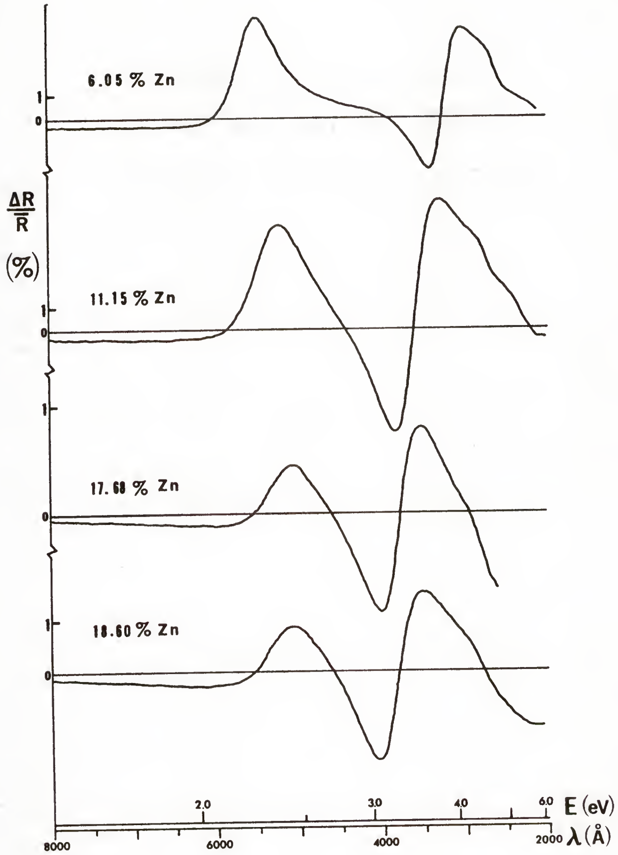
6.05 % Zn
11.15 % Zn
17.68 % Zn
18.60 % Zn
$\frac{\Delta R}{R}$ (%)
1
0
2.0
3.0
4.0
6.0
E (eV)
8000
6000
4000
2000
λ (Å)

Figure 5.3. Differential Reflectograms for various Cu-Al alloys

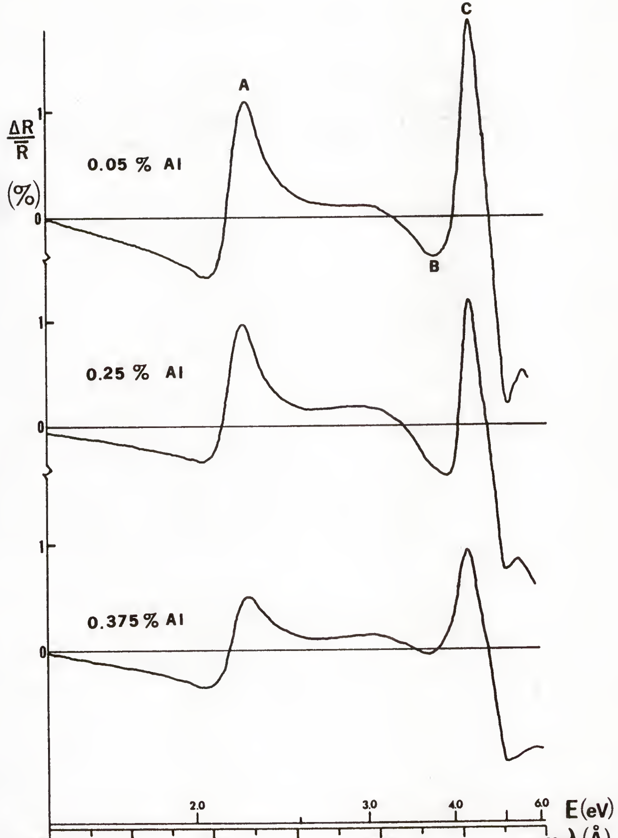
C
A
B
ΔR/R
(%)
1
0
0.05 % Al
1
0
0.25 % Al
1
0
0.375 % Al
2.0
3.0
4.0
6.0
E(eV)
8000
6000
4000
2000
λ(Å)

Figure 5.3 - continued

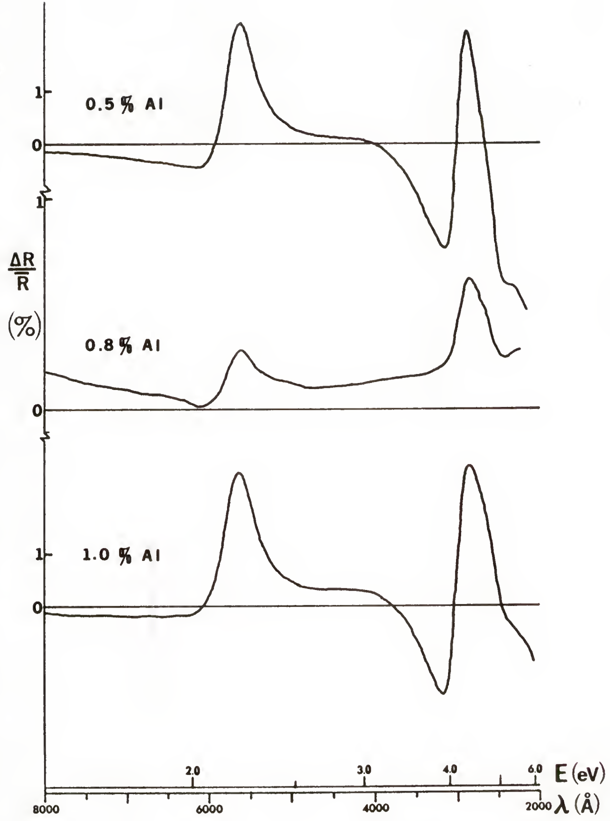
1
0
0.5 % Al
1
ΔR/R
(%)
0.8 % Al
0
1
1.0 % Al
0
2.0
3.0
4.0
6.0
E (eV)
8000
6000
4000
2000
λ (Å)

Figure 5.3 - continued

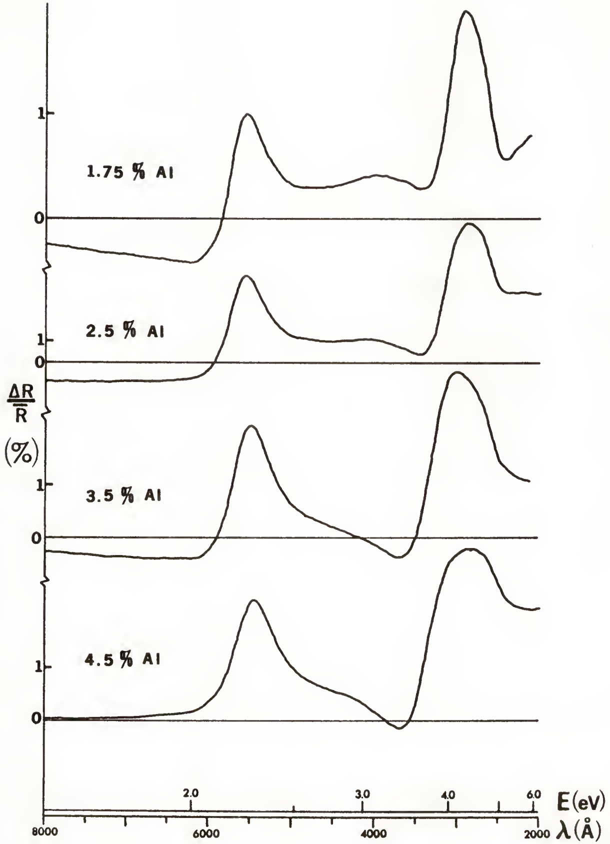
1.75 % Al
2.5 % Al
3.5 % Al
4.5 % Al
1
0
1
0
1
0
1
0
ΔR/R (%)
2.0
3.0
4.0
6.0
E(eV)
8000
6000
4000
2000
λ(Å)

Figure 5.3 - continued

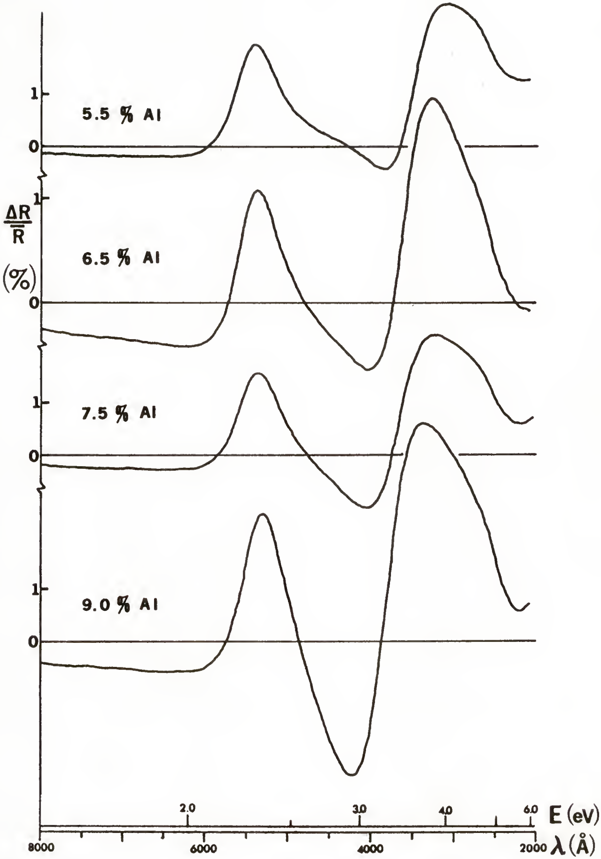
1
5.5 % Al
0
ΔR/R (%)
1
6.5 % Al
0
1
7.5 % Al
0
1
9.0 % Al
0
2.0
3.0
4.0
6.0
E (eV)
8000
6000
4000
2000
λ (Å)

Figure 5.4. Differential Reflectograms for various Cu-Ga alloys

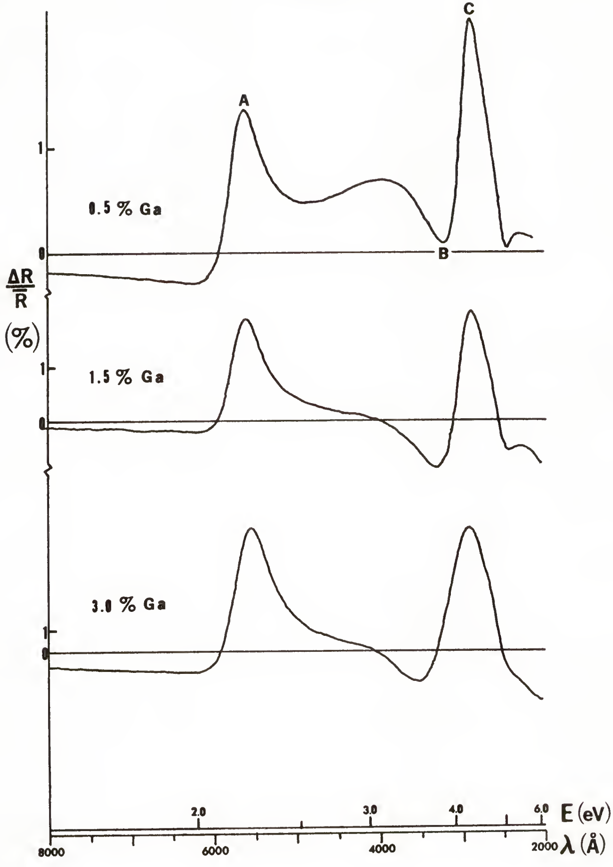
C
A
1
0.5 % Ga
0
B
ΔR/R (%)
1
1.5 % Ga
0
3.0 % Ga
1
0
2.0
3.0
4.0
6.0
E (eV)
8000
6000
4000
2000
λ (Å)

Figure 5.4 - continued

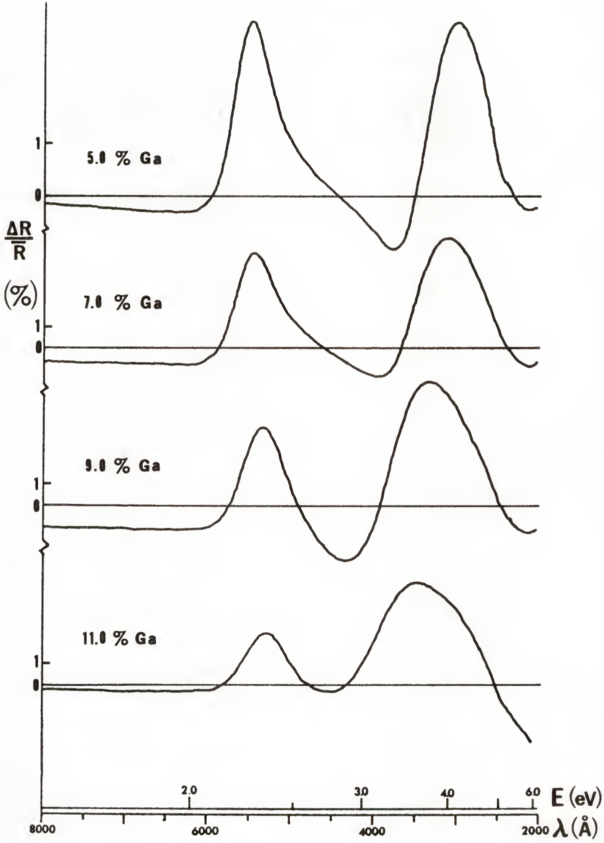

1
5.0 % Ga
0
ΔR/R (%)
7.0 % Ga
1
0
9.0 % Ga
1
0
11.0 % Ga
1
0
2.0
3.0
4.0
6.0
E (eV)
8000
6000
4000
2000
λ (Å)

Figure 5.5. Differential Reflectograms for various Cu-Ge alloys

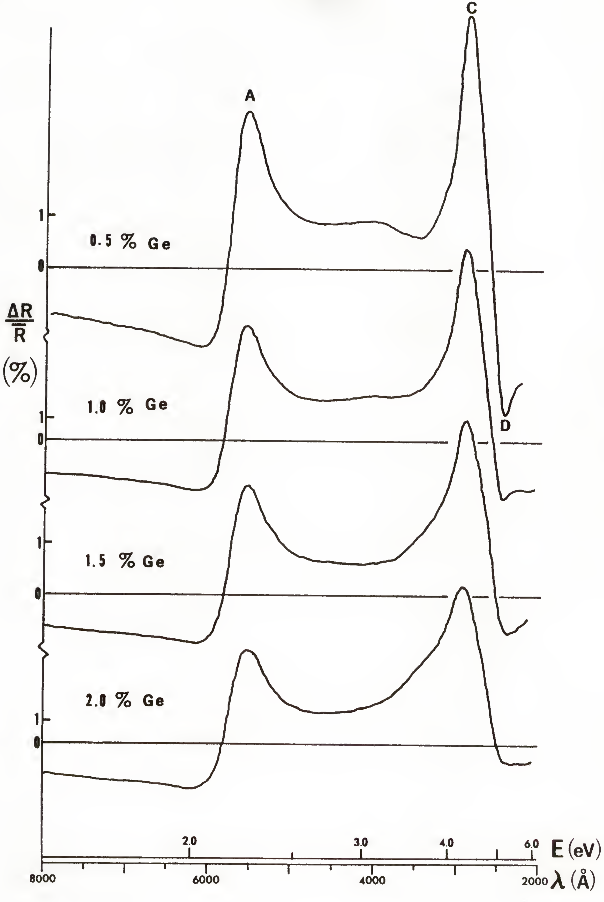
C
A
1
0.5 % Ge
0
ΔR/R
(%)
1.0 % Ge
1
0
D
1
1.5 % Ge
0
2.0 % Ge
1
0
2.0
3.0
4.0
6.0
E (eV)
8000
6000
4000
2000
λ (Å)

Figure 5.5 - continued

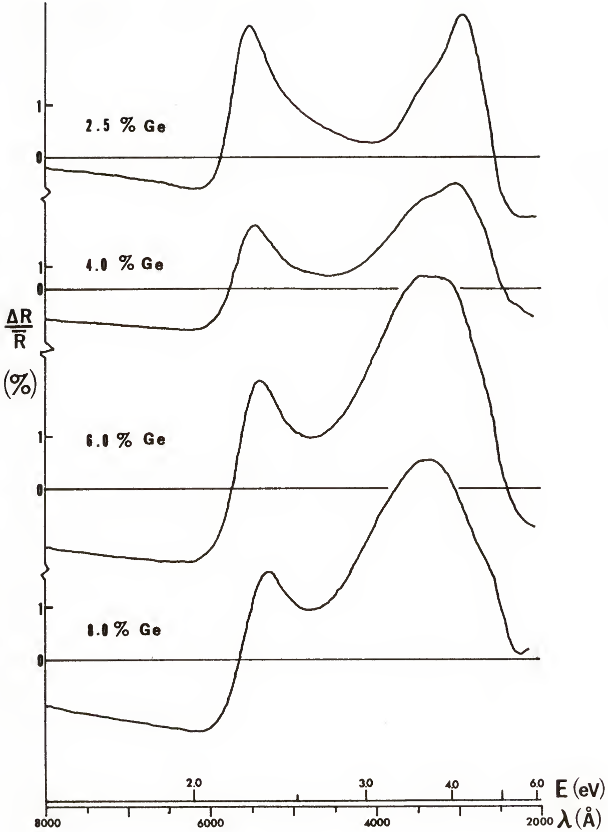
ΔR/R
(%)
1
0
2.5 % Ge
1
0
4.0 % Ge
1
0
6.0 % Ge
1
0
8.0 % Ge
2.0
3.0
4.0
6.0
E (eV)
8000
6000
4000
2000
λ (Å)

Figure 5.6. Differential Reflectograms for various Cu-Si alloys

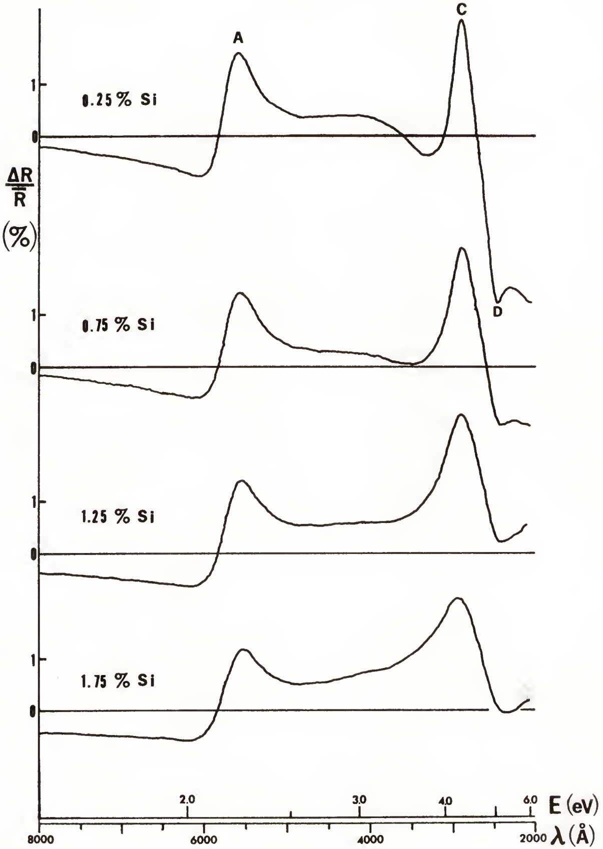
A
C
D
0.25 % Si
0.75 % Si
1.25 % Si
1.75 % Si
1
0
ΔR/R
(%)
2.0
3.0
4.0
6.0
E (eV)
8000
6000
4000
2000
λ (Å)

Figure 5.6 - continued

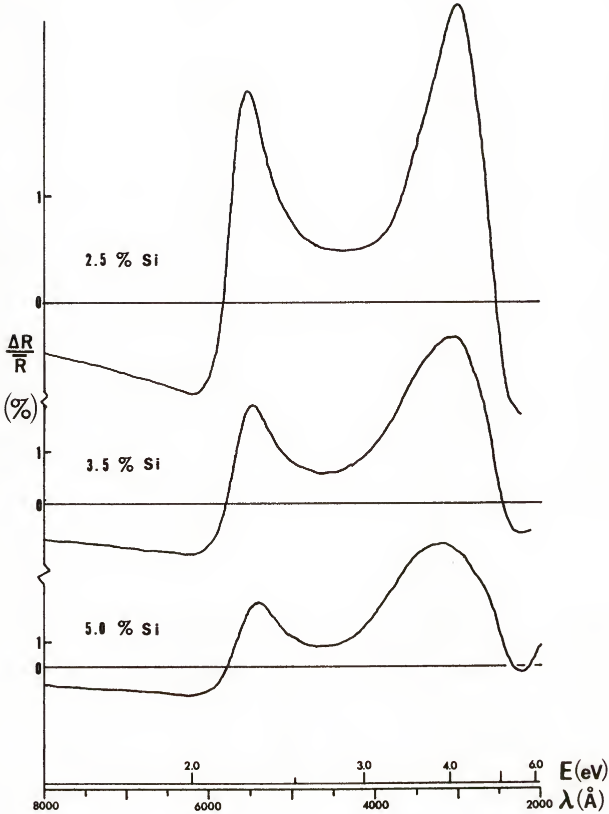
1
2.5 % Si
0
ΔR/R
(%)
1
3.5 % Si
0
5.0 % Si
1
0
2.0
3.0
4.0
6.0
E(eV)
8000
6000
4000
2000
λ(Å)

Figure 5.7. Differential Reflectograms for various Cu-Sn alloys

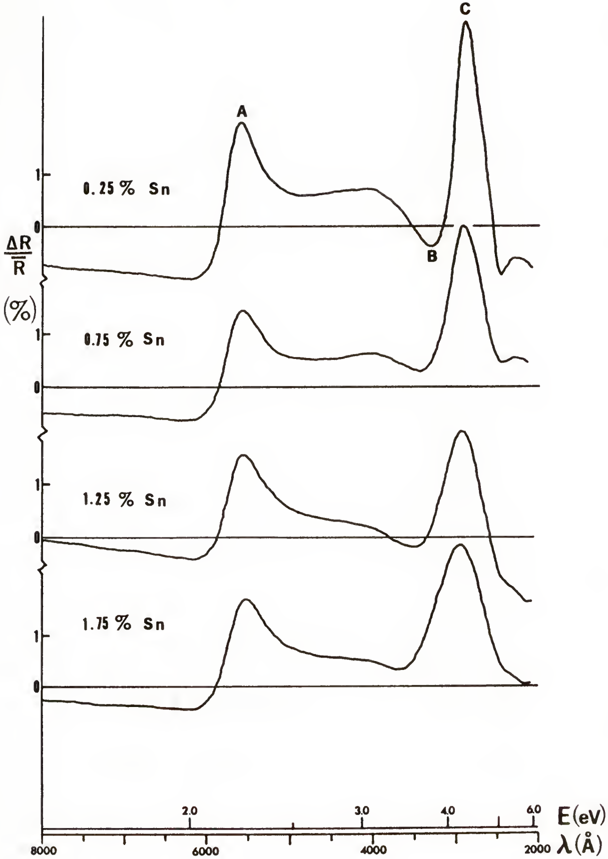
C
A
B
1
0
ΔR/R (%)
0.25 % Sn
0.75 % Sn
1.25 % Sn
1.75 % Sn
2.0
3.0
4.0
6.0
E(eV)
8000
6000
4000
2000
λ(Å)

Figure 5.7 - continued

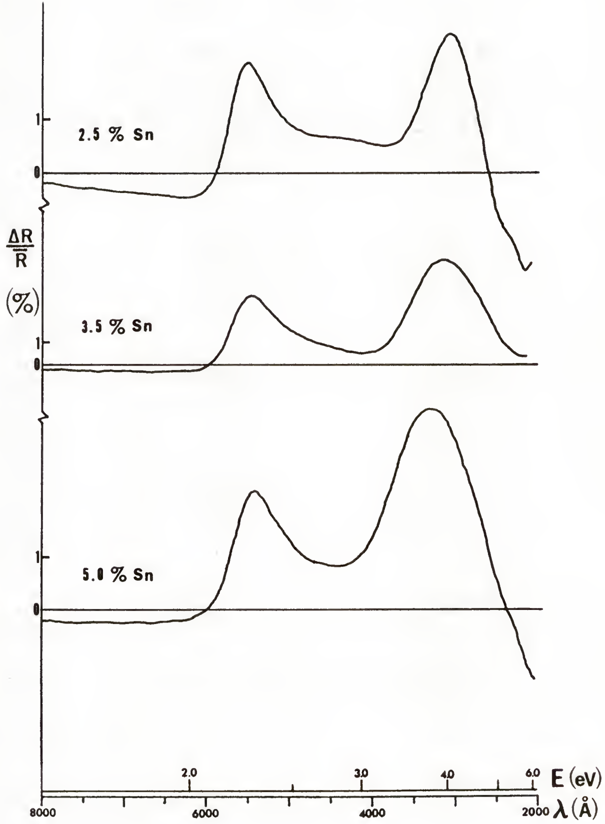
ΔR/R
(%)
1
0
2.5 % Sn
3.5 % Sn
5.0 % Sn
2.0
3.0
4.0
6.0
E (eV)
8000
6000
4000
2000
λ (Å)

Figure 5.8. Differential Reflectograms for various Cu-As alloys

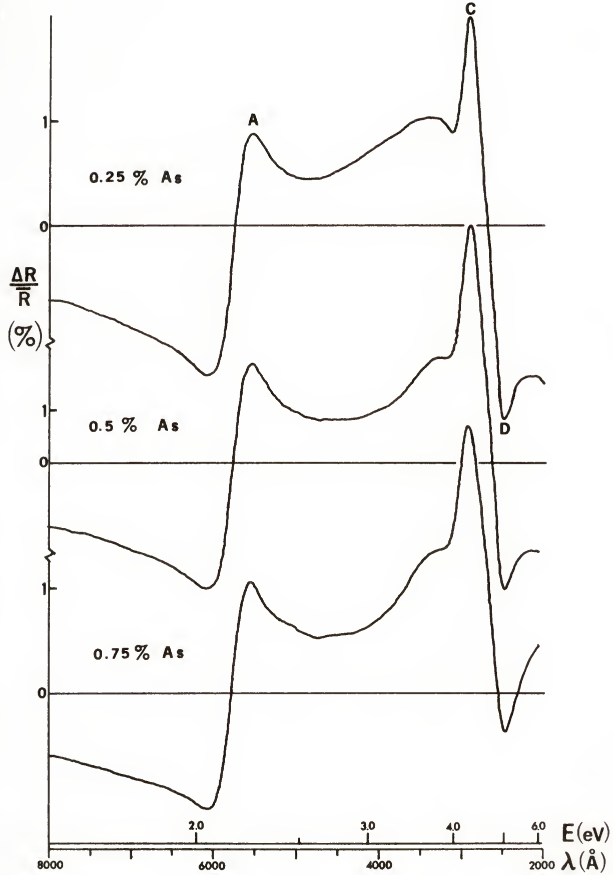
C
A
1
0.25 % As
0
ΔR/R (%)
1
0.5 % As
D
0
1
0.75 % As
0
2.0
3.0
4.0
6.0
E(eV)
8000
6000
4000
2000
λ(Å)

Figure 5.8 - continued

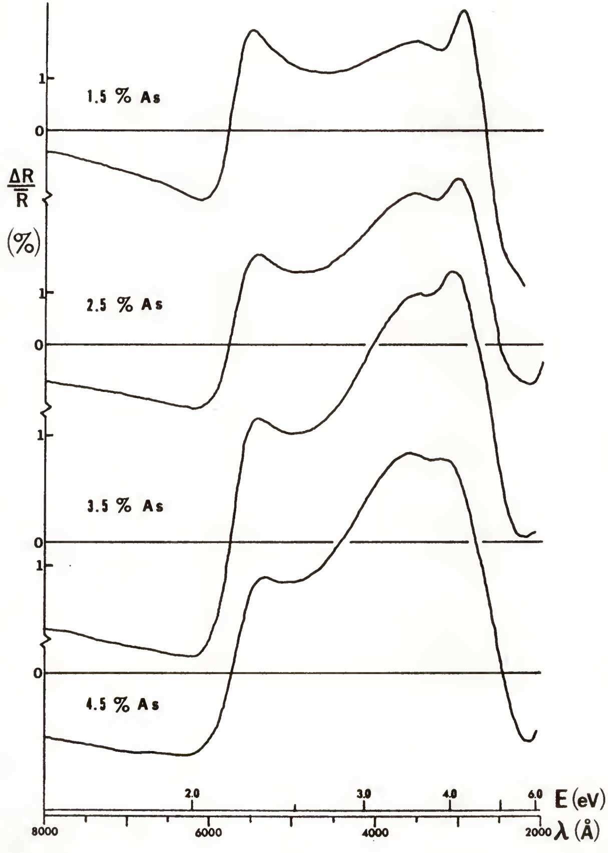
1
1.5 % As
0
ΔR/R
(%)
1
2.5 % As
0
1
3.5 % As
0
1
0
4.5 % As
2.0
3.0
4.0
6.0
E (eV)
8000
6000
4000
2000
λ (Å)

Figure 5.9. Differential Reflectograms for various Cu-Au alloys

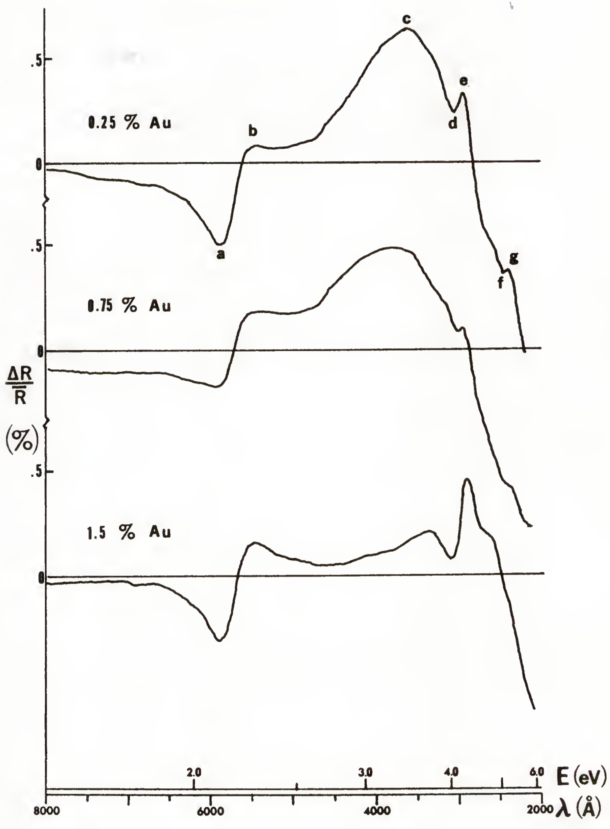
c
.5
e
0.25 % Au
b
d
0
a
.5
g
f
0.75 % Au
0
ΔR/R
(%)
.5
1.5 % Au
0
2.0
3.0
4.0
6.0
E (eV)
8000
6000
4000
2000
λ (Å)

Figure 5.9 - continued

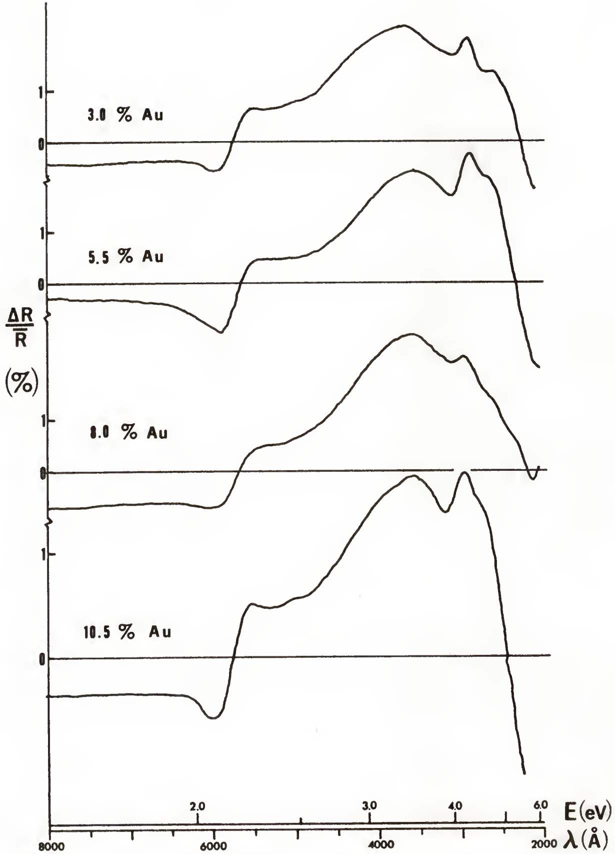
1
3.0 % Au
0
1
5.5 % Au
0
ΔR/R
(%)
1
8.0 % Au
0
1
10.5 % Au
0
2.0
3.0
4.0
6.0
E(eV)
8000
6000
4000
2000
λ(Å)

served, which will be designated as peaks A through D. The energies of these peaks will be presented in the following chapter, along with an analysis and discussion of these results.

CHAPTER VI
DATA ANALYSIS AND DISCUSSION

VI-1 General Remarks

A preliminary assessment of the relevance of the peaks observed in the differential reflectograms of α phase Cu-Zn, Cu-Ge, Cu-Ga, and Cu-Al alloys has been given by Hummel and Andrews.[41] In light of the new line shape analysis of the differential reflectograms which is presented in section IV-3, and due to further experimental and theoretical results presented here and published by others since that time, some fine adjustments to these previous interpretations are given here.

The first section will be concerned with the low energy structure in the differential reflectograms around 2 ev which is widely accepted to be caused by the onset of interband transitions, i.e., the transitions of electrons from the upper d-bands to empty states just above the Fermi energy. The second section will be concerned with the structure between 4 and 5 ev which is observed in the differential reflectograms (and also in conventional optical experiments).

VI-2 Threshold Energy of Interband Transitions

Based on the theory presented in Chapter IV, a fairly accurate description of the implications of the first peak in the differential reflectograms of copper and copper based alloys can be given. It was outlined in detail in section IV-3 that in order to obtain a line shape analysis for peak "A", the derivative of the reflectivity with respect to solute concentration has to be performed, using as an input, transitions from a d-band to the Fermi surface. The derivative indeed provided the shape of a differential reflectogram, reproducing all details around peak "A", so that one can state with reasonable confidence that peak "A" and the substructure around this peak is caused by electron transitions from the d-band to the Fermi energy. However, as shown in section IV-3, the energy of the maximum of peak "A" is not necessarily the energy for this interband transition. Depending on the line shape of the differential reflectograms around peak "A," small corrections have to be performed which amount usually to a few hundredths of an electron volt, i.e., are generally very small. In Table 6.1, the "corrected" transition energies are listed, along with the uncorrected (raw) data.

It should be noted that no corrected data for the Cu-

Table 6.1a

Uncorrected (Raw Data) and Corrected Values for Peak "A" as a Function of Composition for Cu-Zn Alloys

Actual Composition of Alloys [at.%]	Average Composition in [at.%]	E_{Max} Peak "A" [ev]	E_T of Peak "A" (corrected) [ev]
0/0.5	0.25	2.198	2.180
0/1	0.5	2.199	2.182
0/2.5	1.25	2.210	2.187
2.45/7.3	4.88	2.255	2.227
4.8/7.3	6.10	2.269	2.240
9.8/12.5	11.15	2.378	2.343
17.36/18.09	17.73	2.435	2.416
18.2/19	19	2.439	2.413

Table 6.1b

Uncorrected (Raw Data) and Corrected Values for Peak "A" as a Function of Composition for Cu-Al Alloys

Actual Composition of Alloys [at.%]	Average Composition in [at.%]	E_{Max} Peak "A" [ev]	E_T of Peak "A" (corrected) [ev]
0/0.1	0.05	2.219	2.187
0/0.5	0.25	2.214	2.189
0.5/.25	0.375	2.227	2.176
0/1	0.5	2.207	2.185
0.1/1.5	0.80	2.208	2.188
0.5/1.5	1	2.204	2.183
1.5/2	1.75	2.233	2.198
2/3	2.5	2.237	2.208
3/4	3.5	2.263	2.231
4/5	4.5	2.273	2.249
5/6	5.5	2.293	2.267
6/7	6.5	2.309	2.279
7/8	7.5	2.316	2.290
8/10	9	2.344	2.329

Table 6.1c

Uncorrected (Raw Data) and Corrected Values for Peak "A" as a Function of Composition for Cu-Ga Alloys

Actual Composition of Alloys [at.%]	Average Composition in [at.%]	E_{Max} Peak "A" [ev]	E_T of Peak "A" (corrected) [ev]
0/1	0.5	2.210	2.179
1/2	1.5	2.215	2.193
2/4	3	2.236	2.207
4/6	5	2.259	2.233
6/8	7	2.283	2.254
8/10	9	2.326	2.311
10/12	11	2.346	2.331

Table 6.1d

Uncorrected (Raw Data) and Corrected Values for Peak "A" as a Function of Composition for Cu-Si Alloys

Actual Composition of Alloys [at.%]	Average Composition in [at.%]	E_{Max} Peak "A" [ev]	E_T of Peak "A" (corrected) [ev]
0/0.5	0.25	2.216	2.180
0.5/1	0.75	2.223	2.185
1/1.5	1.25	2.236	2.185
1.5/2	1.75	2.245	2.206
2/3	2.5	2.253	2.206
3/4	3.5	2.274	2.233
4/6	5	2.296	2.248

Table 6.1e

Uncorrected (Raw Data) and Corrected Values for Peak "A" as a Function of Composition for Cu-Ge Alloys

Actual Composition of Alloys [at.%]	Average Composition in [at.%]	E_{Max} Peak "A" [ev]	E_T of Peak "A" (corrected) [ev]
0/1	0.5	2.221	2.178
0/2	1	2.232	2.187
1/2	1.5	2.235	2.190
1/3	2	2.245	2.195
2/3	2.5	2.251	2.210
3/5	4	2.277	2.229
5/7	6	2.299	2.242
7/9	8	2.343	2.274

Table 6.1f

Uncorrected (Raw Data) and Corrected Values for Peak "A" as a Function of Composition for Cu-Sn Alloys

Actual Composition of Alloys [at.%]	Average Composition in [at.%]	E_{Max} Peak "A" [ev]	E_T of Peak "A" (corrected) [ev]
0/0.5	0.25	2.219	2.178
0.5/1	0.75	2.226	2.178
1/1.5	1.25	2.231	2.189
1.5/2	1.75	2.246	2.198
2/3	2.5	2.256	2.211
3/4	3.5	2.272	2.226
4/6	5	2.289	2.238

Table 4.1g

Uncorrected (Raw Data) and Corrected Values for Peak "A" as a Function of Composition for Cu-As Alloys

Actual Composition of Alloys [at.%]	Average Composition in [at.%]	E_{Max} Peak "A" [ev]
0/0.5	0.25	2.246
0/1	0.5	2.250
0.5/1	0.75	2.245
1/2	1.5	2.260
2/3	2.5	2.289
3/4	3.5	2.301
4/5	4.5	2.319

As alloys could be obtained in the way as for the other alloys due to the fact that the peak shape in the experimental curves of these alloys are approaching the shape observed for $\Theta \approx 90°$, particularly at low solute concentrations. For higher solute concentrations, they seem to be also distorted by the structure at higher energies (see Figure 5.8).

In Figure 6.1, the corrected transitional energies for peak "A" as a function of average composition for all investigated copper based alloys is plotted. The results can be seen to be qualitatively the same among all these alloy systems: Until slightly above 1 at.%, the solute additions do not vary the threshold energy appreciably from that of pure copper, as has been observed before by Hummel and Andrews.[41] Friedel[2] predicted this type of behavior and related it to "screening" effects. He argued that for the first few atomic percent solute additions to copper, the additional charge from the higher valent solute is effectively screened and the copper matrix behaves as if the impurities were not present. The matrix remains unperturbed and it must thus have the same Fermi level as the pure metal. This remains true as long as the impurities don't interact. After this initial flat portion, the E_T versus composition curve shows, in the

Figure 6.1. Corrected transitional energies for peak "A" as a function of solute concentration for Cu-Zn, Cu-Al, Cu-Ga, Cu-Ge, Cu-Si, and Cu-Sn alloys.
a = possible error in marking maxima
b = possible error introduced by line shape analysis

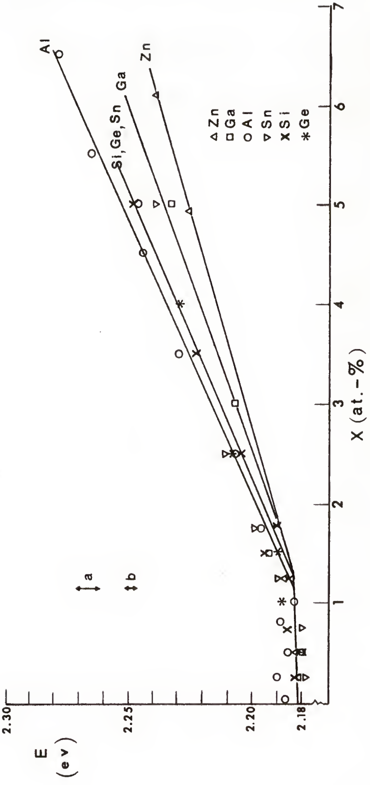
E
(ev)
2.30
2.25
2.20
2.18
X (at.-%)
1
2
3
4
5
6
7
Al
Si,Ge,Sn
Ga
Zn
△ Zn
□ Ga
○ Al
▽ Sn
X Si
* Ge
a
b

present range, a linear increase in energy with increasing solute concentration. It should be noted that these alloys behave very similarly, i.e., the difference in the threshold energies varies only within a few hundredths of an ev. This seems to be an interesting result because it gives some insight into the electron distribution during alloying.

A similar observation was made by Hummel and Andrews[41] on copper based alloys with Zinc, Aluminum, or Gallium, using the peak maxima in the reflectograms as the basis for the transitional energy. With the present, improved differential reflectometer and its higher resolution, a large separation of the behavior of the individual alloy systems could be observed (Figure 6.2). However, with the small corrections of the transitional energies which could be done with the aid of the line shape analysis, the different alloy systems returned to the above mentioned similar E_T versus concentration behavior.

If the Fermi energy were the only parameter in the band structure responding to an increased number of electrons per atom (rigid band model), then all alloy systems would be expected to fall on the same curve in an e/a ratio versus E_T plot. That this is apparently not the case (see Figure 6.3) can be interpreted by the assumption

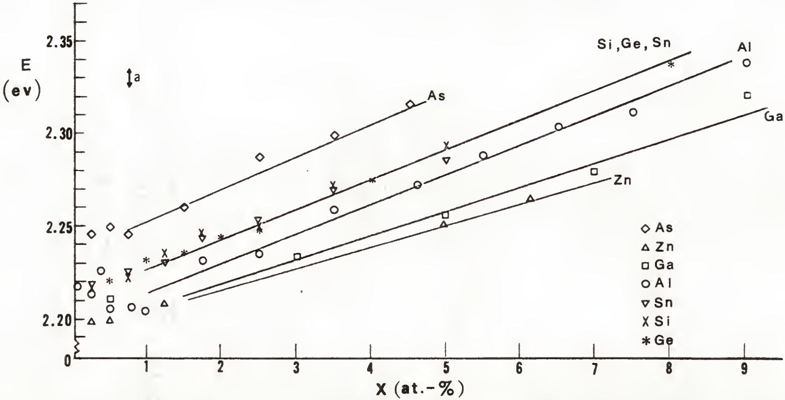

Figure 6.2. Uncorrected transitional energies (raw data) for peak "A" as a function of solute concentration for Cu-Zn, Cu-Al, Cu-Ga, Cu-Ge, Cu-Si, Cu-Sn, and Cu-As alloys.
a = possible error in marking maxima

Figure 6.3. Plot of corrected transitional energies for peak "A" as a function of e/a ratio for Cu-Zn, Cu-Al, Cu-Ga, Cu-Ge, Cu-Si, Cu-Sn, and Cu-As alloys. a = possible error in marking maxima

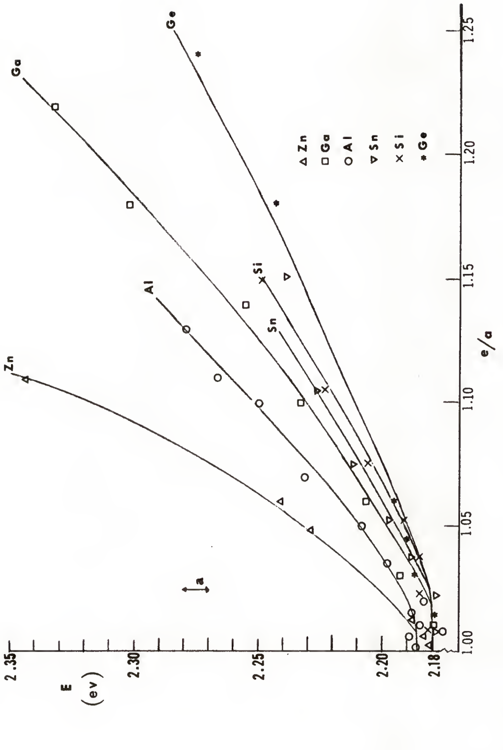
E
(ev)
2.35
2.30
2.25
2.20
2.18
1.00
1.05
1.10
1.15
1.20
1.25
e/a
a
Zn
Al
Sn
Si
Ga
Ge
△ Zn
□ Ga
○ Al
▽ Sn
× Si
* Ge

that the Fermi energy is raised much less than that predicted by the rigid band model. An alternate explanation is that with increasing alloy addition, the d-bands are proportionally raised in energy as was previously suggested by Hummel and Andrews.[41]

Recently, Bansil, Ehrenreich et al.[32] (1974) developed the concept of charge renormalization which arrives from a different point of view to a similar result as the latter suggestion mentioned above. In this theory, it is postulated that when impurities are added to copper, the potential of the copper atoms is modified from that of a neutral atom configuration. These authors demonstrated this on an example: When zinc is alloyed with copper, the copper potential is raised, and as a consequence, the d-bands of copper are also raised in energy. Bansil, Ehrenreich et al. found in addition that both the top and the bottom of the d-bands increase in energy relative to the case with no charge transfer.

A speculation as to why all alloy systems exhibit a similar increase in the transition energy with increasing composition may possibly be the following: It is generally assumed that the Fermi energy increases proportionally as the average number of electrons per atom increases. That is, for a given solute concentration, the Fermi energy is raised more in copper-silicon than in copper-aluminum. However, the amount of charge transfer from silicon to copper can be considered to be greater than that from aluminum to copper, thus increasing the top of the d-bands more for silicon than for aluminum. Thus, by a combination of raising Fermi energy and charge transfer, it is possible to get similar transitional energies for alloys of the same composition. Possible reasons for not obtaining exactly the same transition energy could be due to various mechanisms such as influences of atomic diameter, effective mass, effective number of free electrons, and others.

In summary, the present results in conjunction with recent theories suggest that both the Fermi energy as well as the top of the d-bands increase in energy proportionally with increasing solute concentration in a very specific way so that the actual transitional energies are identical within one or two percent for each alloy having the same solute concentration. The results confirm the predictions of Friedel that up to a solute concentration of about 1 at.%, the additional electrons are effectively screened so that no change in the electronic configuration occurs in this concentration range.

VI-3 High Energy Structure in the Differential Reflectograms

VI-3.1 Transition Around 5 ev

The line shape analysis of peak "A" discussed in Chapter IV implied transitions from the d-bands to the Fermi energy. It is widely agreed in the literature[12,17,25-28] that absorption around 5 ev can be identified from the optical spectra which also involves transitions from the d-bands to the Fermi energy. However, in this case, the transitions are suggested to originate from the lower d-bands instead of from the upper ones.

It is therefore considered to be appropriate to employ a similar line shape analysis for the observed structure around 5 ev. One has to keep in mind, however, that in this energy region, α is negative and β is positive (Figure 6.4), so that the β/α ratio is negative. This is contrary to the condition around 2 ev where β/α is positive. The negative β/α ratio around 5 ev results therefore in a line shape which is inverted compared to the one for peak "A," i.e., one has to expect an "up-down" line shape. (See in this context, Figure 4.4; Θ between 180° and 270°.) This type of line shape can indeed be observed in differential reflectograms at energies around 5 ev involving peaks "C" and "D." To investigate this

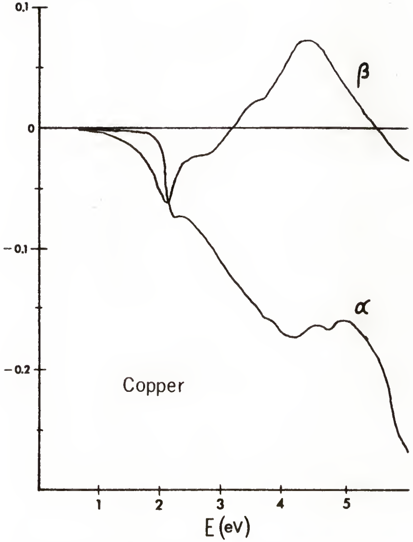

Figure 6.4. The Seraphin coefficients α and β for copper

further, it is desirable to select an alloy system in which the 5 ev peak dominates over other structure in the vicinity. Pells and Montgomery[17] have shown that this is the case for Cu-As and, to a certain extent, also for Cu-Ge (see Figures 2.7c and d). In these alloy systems, the "high energy" peak (around 5 ev) was observed to be much stronger than the so called "low energy" peak around 4 ev.

By inspecting the various differential reflectograms for Cu-Ge, Cu-Si, and Cu-As alloys (Figures 5.5, 5.6 and 5.8), a pronounced structure in the form of a maximum "C" can be seen which is closely followed by a sharp minimum "D." This type of behavior cannot be seen in the differential reflectograms for Cu-Zn, for which alloys, according to Pells and Montgomery, the "low energy" peak around 4 ev is predominant. The differential reflectograms of these alloys confirm, therefore, qualitatively the observations which were obtained from conventional optical data. The considerations above lead to the conclusion that pertinent information about the behavior of the "high energy" peak around 5 ev can be conveniently deduced from the differential reflectograms for Cu-Ge, Cu-Si, and Cu-As. One has to take into account, however, that the situation may be complicated by the close vicinity of a possible "low energy" peak, which influences the location of the maximum "C." Parallel to the reasoning given in Chapter IV for the line shape analysis of the 2 ev peak, one can argue that the basic information about this 5 ev peak is contained in the minimum "D," and that similarly as for the 2 ev peak, a small correction has to be applied to obtain the correct transition energy. From the experience presented in the previous section, it can be assumed that this correction must be very small. Therefore, the actual transition energy is expected to be a few hundredths of an electron volt smaller than the energy of peak "D."

Since we are basically interested in the energy shifts due to alloying, this minimum "D" will be considered only in the following analysis. Both Table 6.2 and Figure 6.5 present the energies of peak "D" and the energy shifts compared to "pure copper" as a function of composition for the Cu-Ge, Gu-Si, and Cu-As alloys. (The "pure copper" point was obtained by extrapolating the curve to X = 0.) It can be seen then that the energy difference increases with increasing solute concentration. This behavior is similar to that observed for the upper d-band → Fermi energy transition (see Figure 6.1), and can be interpreted similarly by considering that the Fermi energy is raised with increasing solute concentration. As

Table 6.2

Energy of Peak "D" and Shift in Energy as a Function of Composition for Various Copper Based Alloys

Average Composition of Alloy [at.%]	Energy of Peak "D" [ev]	Shift in Energy Compared to Pure Copper [ev]
Cu - 0.25 at.% Ge	5.06	0.03
Cu - 1 at.% Ge	5.06	0.03
Cu - 1.5 at.% Ge	5.16	0.13
Cu - 0.25 at.% Si	5.03	0
Cu - 0.75 at.% Si	5.08	0.04
Cu - 1.25 at.% Si	5.09	0.06
Cu - 1.75 at.% Si	5.30	0.27
Cu - 3.50 at.% Si	5.57	0.54
Cu - 0.25 at.% As	5.04	0.01
Cu - 0.50 at.% As	5.06	0.03
Cu - 0.75 at.% As	5.06	0.03
Cu - 2.50 at.% As	5.77	0.74
Cu - 3.50 at.% As	5.67	0.64
Cu - 4.50 at.% As	5.80	0.77

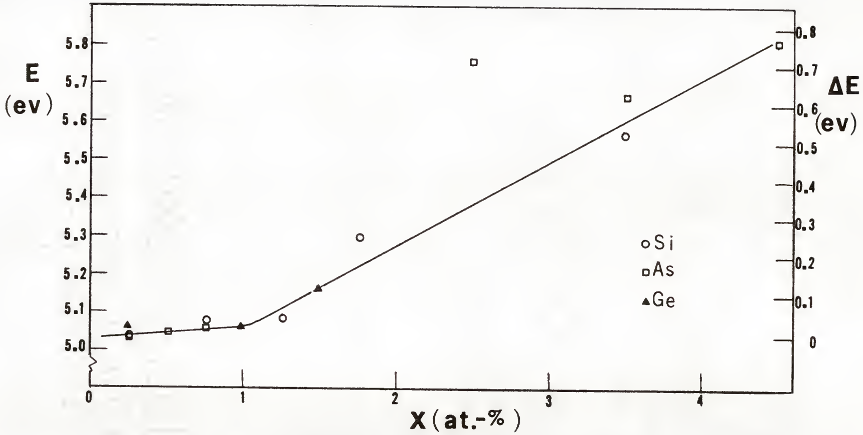

Figure 6.5. Energy of peak "D" and shift in energy compared to "pure copper" as a function of composition for various copper-based alloys

for the threshold energy, practically no shift in energy can be observed up to about 1 at.% solute, which possibly confirms that indeed the Fermi energy is involved in this transition. Particular attention should be given to the fact that the threshold energy (upper d-bands → E_F transition) rises as an average only 1.2×10^{-2} ev per at.% solute, whereas the present transition (lower d-bands → E_F) rises by about 16×10^{-2} ev per at.% solute, i.e., more than ten times as much. Since the rise in Fermi energy is, of course, the same in both cases, the difference can only be attributed to a difference in the behavior of the upper compared to the lower d-bands. In the previous section, we attributed the unexpectedly small shift of the threshold energy, E_T, with increasing solute concentration to the rise of the upper d-bands. Our above mentioned results for the lower d-bands to E_F transition seem to indicate, in contrast to this, that the lower d-bands are either not affected at all by alloying or move only small amounts. In any event, the contrasting results for transitions from the lower and from the upper d-bands seem to confirm that the upper d-bands are indeed raised by alloying as proposed in the previous section and suggested by Bansil *et al.* from their calculations.

VI-3.2 Transition Around 4 ev

As pointed out in Chapter II, it is widely assumed that the structure around 4 ev which is found in conventional as well as in modulated optical spectra is due to interband transitions between two "conduction bands," for example from $L_{2'}$ to L_1. Due to this fact, the line shape analysis presented in Chapter IV, which used as a basis d-band to Fermi energy transitions, cannot be used here. A line shape analysis for these transitions seems to be more involved. Therefore, a different, that is, an empirical approach has to be employed for the discussion of these transitions.

By plotting the position of peaks "B" and "C" versus solute concentration for Cu-Zn (Figure 6.6), it can be seen that both curves run essentially parallel to each other. This suggests that the same information is contained in both peaks "B" and "C." Pells and Montgomery[17] infer from their experiments that in Cu-Zn alloys, a predominance of the "low energy" peak (i.e., the peak around 4 ev) is present. This is confirmed by the differential reflectograms for these alloys. It can be seen in these reflectograms (Figure 5.2) that peaks "B" and "C" are strongly pronounced, whereas peak "D" is only weakly visible in the form of a small deviation from an otherwise smooth curve.

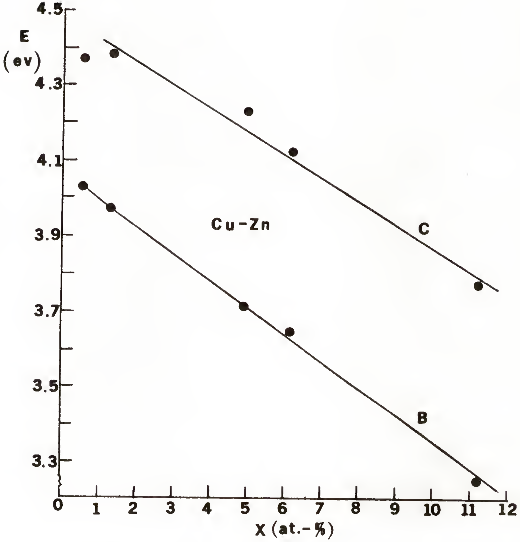

Figure 6.6. Energy of peaks "B" and "C" vs. solute concentration for Cu-Zn alloys

The information about the shift of the "low energy" peak with alloy composition can therefore be considered to be contained in peak "B" and also to a certain extent in peak "C," inasmuch as peak "C" is not influenced by the "high energy" transition around 5 ev, as for example in Cu-As alloys.

The energy change of peak "B" with respect to increasing alloy concentration for various copper alloys can be found in Table 6.3 and Figure 6.7. It can be seen there that the energy of peak "B" decreases sharply with increasing solute concentration, as observed before by several investigators,[15-17,23,24,26,29,30,32,40] for the transitions around 4 ev, and also predicted through several band calculations for the conduction band to conduction band transition ($L_{2'} \rightarrow L_1$). It should be noted from Figure 6.7 that the decrease in the transitional energy is much larger in Cu-Ga or Cu-Al alloys, compared to Cu-Zn, and that Cu-Sn reveals an even larger decrease compared to Cu-Ga or Cu-Al. It also appears significant that the behavior is alike for both Cu-Ga and Cu-Al alloys which possess identical electron concentrations per atoms. This seems to indicate that the shift of the energies is strongly influenced by the electron concentration of the solute. Further discussions have to await detailed band calculations which take into account the change in the conduction bands due to alloying.

Table 6.3a

Energy of Peak "B" as a Function of Solute Concentration for Cu-Zn Alloys

Actual Composition of Alloys [at.%]	Average Composition of Alloys [at.%]	Energy of Peak "B" [ev]
0/0.5	0.25	4.319
0/1	0.5	4.036
0/2.5	1.25	3.972
2.45/7.3	4.88	3.716
4.8/7.3	6.10	3.651
9.8/12.5	11.15	3.250

Table 6.3b

Energy of Peak "B" as a Function of Solute Concentration for Cu-Al Alloys

Actual Composition of Alloys [at.%]	Average Composition of Alloys [at.%]	Energy of Peak "B" [ev]
0/0.1	0.05	3.717
0/0.5	0.25	3.932
0/1	0.5	3.939
0.5/1.5	1	3.924
1.5/2	1.75	3.619
2/3	2.5	3.595
3/4	3.5	3.361
4/5	4.5	3.351
5/6	5.5	3.256

Table 6.3c

Energy of Peak "B" as a Function of Solute Concentration for Cu-Ga Alloys

Actual Composition of Alloys [at.%]	Average Composition of Alloys [at.%]	Energy of Peak "B" [ev]
0/1	0.5	3.834
1/2	1.5	3.760
2/4	3	3.526
4/6	5	3.292
6/8	7	3.176
8/10	9	2.876
10/12	11	2.756

Table 6.3d

Energy of Peak "B" as a Function of Solute Concentration for Cu-Sn Alloys

Actual Composition of Alloys [at.%]	Average Composition of Alloys [at.%]	Energy of Peak "B" [ev]
0/0.5	0.25	3.794
0.5/1	0.75	3.620
1/1.5	1.25	3.535
1.5/2	1.75	3.377
2/3	2.5	3.274
3/4	3.5	3.103
4/6	5	2.819

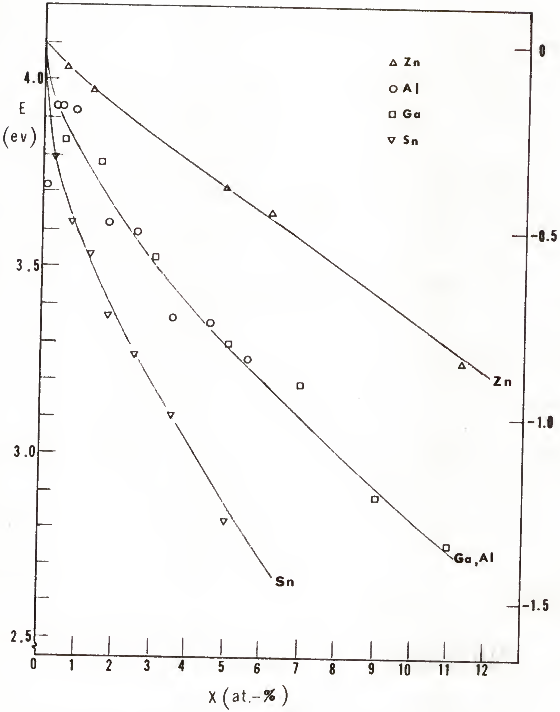

Figure 6.7. Energy of peak "B" and shift in energy compared to "pure copper" as a function of composition for various copper-based alloys

VI-4 Cu-Au Alloys

VI-4.1 General Remarks

In this section, the discussion of the copper-gold alloys is treated because they possess somewhat different features than the other alloy systems (see Figure 5.9).

VI-4.2 Threshold Energy for Interband Transitions

The threshold energy for the transitions from the top of the d-bands to the Fermi energy can be taken, as in section VI-2, from the structure in the differential reflectograms around 2 ev. As in that section, the maximum "b" is taken as the threshold energy, even though this peak is less pronounced in Cu-Au (Figure 5.9). By comparing the various line shapes (Figure 4.3) with the Cu-Au differential reflectograms, it can be inferred that the Cu-Au line shape is similar to the theoretical curves for $\Theta \approx 60°$. It has to be kept in mind that, as before, a correction for the true E_T should be undertaken, which will decrease the energy of peak "b" slightly. However, because of the flat tail toward higher energies, the correction technique used in Chapter IV cannot be applied here. This is, nevertheless, of little significance since we are basically interested in energy shifts only.

In Figure 6.8, the energy of peak "b" is plotted versus the average composition of the alloy. It can be seen that, within the reading error of the maxima, the threshold energy for interband transitions is not changed by gold additions to copper. This behavior is expected since both copper and gold have the same valence electron concentration. This means that by replacing Cu atoms with Au atoms, the Fermi energy, as well as the top of the d-bands of copper, remain unchanged in accordance with the rigid band model.

VI-4.3 Lower d-bands to Fermi Energy Transitions

As in section VI-3.1, an energy for the lower d-band to Fermi energy transition can be deduced from the differential reflectograms out of peaks "f" and "g" (Figure 5.9), which are, as before, around 5 ev. It seems to be significant that these transitions become weaker with increasing Au concentration, as can be inferred from the disappearance of the structure around 5 ev at higher Au concentrations.

VI-4.4 Conduction Band to Conduction Band Transitions

Another structure around 4 ev can be observed in the reflectograms (peaks "d" and "e"). Similarly, as in sec-

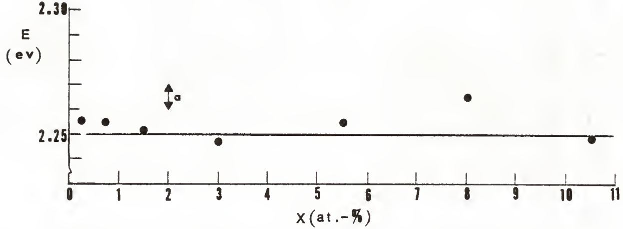

Figure 6.8. Energy of peak "b" as a function of composition for Cu-Au alloys.
a = possible error in marking maxima

tion VI-3.2, this structure is interpreted to be caused by conduction band to conduction band transitions. In Figure 6.9, the shift in energy of these transitions can be followed using the minima (peak "d"). Also from this figure, it can be seen that, with increasing gold concentration, the transitional energy decreases. This shift is much smaller than that observed for the same transition in Cu-Zn and similar alloys.

VI-4.5 Broad Structure

The differential reflectograms (Figure 5.9) show a broad structure around 3 ev. This structure can be considered to be the result of several, closely spaced interband transitions which cannot be individually resolved. For the interpretation of this structure, it should be kept in mind that some of the gold d-bands lie in the same energy interval as the copper d-bands, so that additional interband transitions, originating from the Au d-bands, are possible. This may cause the structure around 3 ev which is not observed in Cu-Zn, for example.

In Figure 6.10, the shift of the maximum of this structure is plotted. It can be seen that the maximum "c" increases substantially with increasing gold concentration.

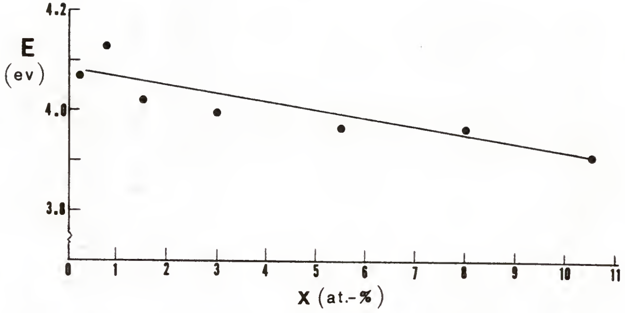

Figure 6.9. Energy of peak "d" as a function of composition for Cu-Au alloys

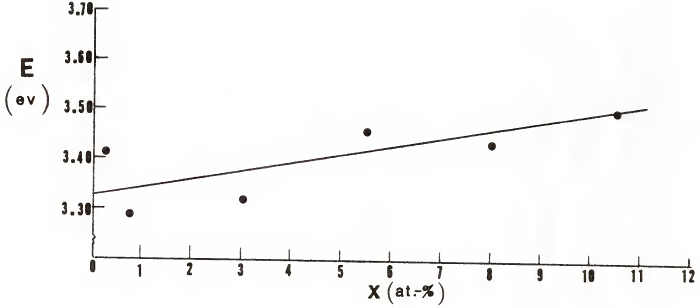

Figure 6.10. Energy of peak "c" as a function of composition for Cu-Au alloys

In summary, it was observed that Cu-Au alloys behave, in many respects, as expected. Optical investigations of these alloys are an interesting supplement to the studies of the alloy systems reported in the previous sections in which the electron concentration has been gradually increased.

APPENDIX 1

Proof that

$$\frac{\Delta R}{R} = \alpha\frac{d\varepsilon_1}{dx} + \beta\frac{d\varepsilon_2}{dx} = \mathrm{Re}\{ce^{i\Theta}\ \frac{d\hat{\varepsilon}}{dx}\}:$$

$$\hat{\varepsilon} = \varepsilon_1 - i\varepsilon_2$$

$$\frac{d\hat{\varepsilon}}{dx} = \{\frac{d\varepsilon_1}{dx} - i\frac{d\varepsilon_2}{dx}\}$$

It follows for Equation (27) with $\alpha + i\beta = ce^{i\Theta}$ that

$$\frac{\Delta R}{R} = \mathrm{Real}\{(\alpha + i\beta) \cdot (\frac{d\varepsilon_1}{dx} - i\frac{d\varepsilon_2}{dx})\}$$

and

$$\frac{\Delta R}{R} = \mathrm{Real}\{\alpha\frac{d\varepsilon_1}{dx} + \beta\frac{d\varepsilon_2}{dx} + i\beta\frac{d\varepsilon_1}{dx} - i\alpha\frac{d\varepsilon_2}{dx}\}$$

Therefore,

$$\frac{\Delta R}{R} = \alpha\frac{d\varepsilon_1}{dx} + \beta\frac{d\varepsilon_2}{dx}$$

APPENDIX 2

Definition of a complex quantity:

$$\hat{A} = a + ib \quad \text{and} \quad a + ib = \rho e^{i\Theta}$$

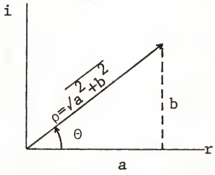

$$a + ib = \sqrt{a^2 + b^2}\; e^{i\Theta}$$

Let $a = s$
$b = 1$
$\Theta = \phi$

Define $s = \dfrac{\omega-\omega_T}{\Gamma}$

Since $s + i = \sqrt{s^2 + 1}\; e^{i\phi}$, one obtains

$$\frac{i}{s+i} = \frac{i}{\sqrt{s^2+1}}\, e^{-i\phi}$$

and knowing that $i = e^{i\pi/2}$

$$\frac{i}{s+i} = \frac{1}{\sqrt{s^2+1}}\, e^{i(\frac{\pi}{2}-\phi)}$$

LIST OF REFERENCES

1. N. F. Mott and H. Jones, The Theory of the Properties of Metals and Alloys, Clarendon Press, Oxford, 1936, p. 119.

2. J. Friedel, Proc. Phys. Soc. (London), B65 (1952) 769.

3. M. A. Biondi and J. A. Rayne, Phys. Rev., 115 (1959) 1522.

4. B. Segall, Phys. Rev., 125 (1962) 109.

5. H. Ehrenreich and H. R. Philipp, Phys. Rev., 128 (1962) 1622.

6. C. N. Berglund and W. E. Spicer, Phys. Rev., 136 (1964) A1030.

7. W. E. Spicer, Phys. Letters, 20 (1966) 325.

8. B. R. Cooper, H. Ehrenreich and H. R. Philipp, Phys. Rev., 138 (1965) A494.

9. D. Beaglehole, Proc. Phys. Soc., 87 (1966) 461.

10. U. Gerhardt, D. Beaglehole and R. Sandrock, Phys. Rev. Letters, 19 (1967) 309.

11. U. Gerhardt, Phys. Rev., 172 (1968) 651.

12. F. M. Mueller and J. C. Phillips, Phys. Rev., 157 (1967) 600.

13. G. Dresselhaus, Solid State Commun., 7 (1969) 419.

14. M. M. Pant and S. K. Joshi, Phys. Rev., 180 (1969) 675.

15. A. Lettington, Phil. Mag., 11 (1965) 863.

16. H. Amar, K. H. Johnson and C. B. Sommers, Phys. Rev., 153 (1967) 655.

17. G. P. Pells and H. Montgomery, J. Phys. C. Suppl. Met. Phys., 3 (1970) 330.

18. P. Soven, Phys. Rev., 151 (1966) 539.

19. C. Y. Fong, M. L. Cohen, R. R. L. Zucco, J. Stokes and Y. R. Shen, Phys. Rev. Letters, 25 (1970) 1486.

20. M. Welkowsky and R. Braunstein, Solid State Commun., 9 (1971) 2139.

21. A. R. Williams, J. F. Janak and V. L. Moruzzi, Phys. Rev. Letters, 28 (1972) 671.

22. P. B. Johnson and R. W. Christy, Phys. Rev. B, 6 (1972) 4370.

23. M. P. Das and S. K. Joshi, J. Phys. F, 2 (1972) L42.

24. R. E. Hummel and J. B. Andrews, Phys. Rev. B, 8 (1973) 2449.

25. A. S. DeReggi and R. S. Rea, Phys. Rev. Letters, 30 (1973) 549.

26. R. S. Rea and A. S. DeReggi, Phys. Rev. B, 9 (1974) 3285.

27. R. Rosei and D. W. Lynch, Phys. Rev. B, 5 (1972) 3883.

28. D. Beaglehole and E. Erlbach, Phys. Rev. B, 6 (1972) 1209.

29. D. Beaglehole, Surf. Sci., 37 (1973) 708.

30. D. Beaglehole and M. Wihl, Solid State Commun., 13 (1973) 427.

31. T. Suzuki, M. Hasegawa and M. Hirabayashi, Appl. Phys., 5 (1974) 269.

32. A. Bansil, H. Ehrenreich, L. Schwartz and R. E. Watson, Phys. Rev. B, 9 (1974) 445.

33. R. E. Hummel, J. A. Holbrook and J. B. Andrews, Surf. Sci., 37 (1973) 717.

34. J. A. Holbrook and R. E. Hummel, Rev. of Sci. Instruments, 44 (1973) 463.

35. R. E. Hummel, *Optische Eigneschaften von Metallen und Legierungen*, Springer Verlag, 1971.

36. F. Stern in *Solid State Physics*, Vol. 15, eds., F. Sietz and D. Turnbull, Academic Press, Inc., New York, 1963, pp. 327-408.

37. B. O. Seraphin in *Optical Properties of Solids*, ed., F. Abelès, North-Holland Publishing Company, 1972, pp. 164-276.

38. R. Enderlein, private communication, 1975.

39. J. A. Holbrook, Ph.D. Dissertation, University of Florida, 1972.

40. J. B. Andrews, Ph.D. Dissertation, University of Florida, 1974.

41. R. E. Hummel and J. B. Andrews, Phys. Rev., 8 (1973) 2449.

BIOGRAPHICAL SKETCH

Rosalia Josephine Nastasi was born July 1, 1948, in New York, New York. She attended Hornell Senior High School in Hornell, New York, where she graduated in 1966. From 1966 to 1970, the author studied at Alfred University in Alfred, New York, where she graduated with a Bachelor of Science degree in Ceramic Science. Miss Nastasi entered graduate school at the Pennsylvania State University in 1970 and graduated in 1972 with a Master of Science degree in Ceramic Science. The author entered graduate school at the University of Florida in September, 1972, in the field of Materials Science and Engineering. She received the degree of Master of Science in March, 1975, and has pursued the degree of Doctor of Philosophy since that date.

The author is a member of the American Institute of Mining, Metallurgical and Petroleum Engineers, the American Society for Metals, Alpha Sigma Mu, The American Ceramic Society, Keramos, and the Engineering Leadship Circle.

I certify that I have read this study and that in my opinion it conforms to acceptable standards of scholarly presentation and is fully adequate, in scope and quality, as a dissertation for the degree of Doctor of Philosophy.

R C Hummel

Rolf E. Hummel, Chairman
Professor of Materials Science
and Engineering

I certify that I have read this study and that in my opinion it conforms to acceptable standards of scholarly presentation and is fully adequate, in scope and quality, as a dissertation for the degree of Doctor of Philosophy.

John J Hren

John J. Hren
Professor of Materials Science
and Engineering

I certify that I have read this study and that in my opinion it conforms to acceptable standards of scholarly presentation and is fully adequate, in scope and quality, as a dissertation for the degree of Doctor of Philosophy.

R. T. DeHoff for D.B. Dove

Derek B. Dove
Professor of Materials Science
and Engineering

I certify that I have read this study and that in my opinion it conforms to acceptable standards of scholarly presentation and is fully adequate, in scope and quality, as a dissertation for the degree of Doctor of Philosophy.

R. Pepinsky

R. Pepinsky
Professor of Physics

This dissertation was submitted to the Graduate Faculty of the College of Engineering and to the Graduate Council, and was accepted as partial fulfillment of the requirements for the degree of Doctor of Philosophy.

August, 1976

Dean, College of Engineering

Dean, Graduate School